Chapter 4

Development of multifunctional fluorescence-emitting theranostic agents

Chapter 4

Development of multifunctional fluorescence-emitting theranostic agents

4.1 Design strategy

Theranostic fluorescence probes can simultaneously perform the detection of Aβ aggregates and inhibit the cholinesterase enzymes, which are primary targets for the design and development of therapeutics for AD. A novel series of theranostic agents have been designed with the amalgamation of the structural features from the potential anti-AD agents and fluoroprobes with the architecture of electron donor-acceptor (113). The development of a promising theranostic agent requires a rational structural framework combination containing two major functionalities including, a lead structural scaffold from existing therapeutics and biomarker labeling agents. The potential theranostic agents have been designed with the incorporation of key structural features from the anti-AD therapeutic classes and fluoroprobes (AD-biomarkers labeling agents) based on the previously obtained results in our laboratory and available literatures **(Figure 4.1)**. The intramolecular charge transfer (ICT) type of the fluorescent probes can be constructed through the architecture of molecules with three main structural fragments including, electron-acceptor group, conjugated degree of the "π-electron bridge", and electron-donor group (27). The modification or alteration in the electron-donor and acceptor groups increase or decrease in the degree of conjugation of the π bridge significantly and affects the optical and biological properties of probes including emission wavelength (λ_{em}), quantum yield (Φ), target affinity and BBB permeability (114). The novel ICT type, 1, 3-dimethylbarbituric acid-based *N*-aryl piperazine bearing scaffold was constructed through incorporation of the structural features from the potential anti-AD agents and the architecture of electron donor-acceptor with π bridge **(Figure 4.1)**. The presence of pseudoaromatic pyrimidine-2,4,6-trione ring in the barbituric acid was employed as an electron-withdrawing moiety in the construction of classic push–pull chromophores (115, 116). Several studies demonstrated the potential of barbituric

acid scaffold to quantify the Aβ species *in vitro* and *in vivo* studies (117). Zhou *et al.* reported the NIRF probe, **BBTOM-3** for Aβ imaging using barbituric acid moieties as acceptors, where the planar geometry makes a significant contribution to the binding affinity for Aβ aggregates with longer emission wavelengths (118). Wang E. *et al.* designed the red-emissive barbituric acid-functionalized tetraphenylethene derivative (**TPE-HPh-Bar**) which exhibits the effect of twisted intramolecular charge transfer (TICT) due to the interaction of its donor and acceptor units and demonstrated the aggregation-induced emission phenomenon (119). Adibi H. *et al.* reported the barbituric and thiobarbituric acid based chromene derivatives, as new fluorescent dyes to detect quantitatively amyloid fibrils. Compound **4a** showed the high binding affinity to amyloid fibrils in dye-binding studies based on selectivity and specificity parameters (117). Therefore, we have incorporated the planar 1, 3-dimethylbarbituric acid moiety as stronger acceptors to obtain a higher affinity for Aβ aggregates and longer emission wavelength. The conjugated π-electron containing benzylidene moiety was employed as the backbone structure to bridge the donor−acceptor architecture. It could induce a redshift in both absorption and emission spectra. Further, *N*, *N*-dimethylamino group is reported as an ideal electron-donor, and plays an important role in recognizing the β-sheet structure (120). The strong electron-donating ability of *N, N′*-dimethylamino substituent have been widely studied. **Probe 4b** was designed in a way to undergo the mechanism of TICT and showed a strong affinity towards Aβ aggregates with a "turn-on" fluorescence effect upon interaction and a remarkable increase in the intensity along with the change in emission wavelength (65). The presence of *N*, *N*-dimethylamino group in the piperazine scaffold makes it bifunctional electron-donor systems (121). Youngmin *et al.* reported a series of fluorescent probes targeting Aβ, based on a donor−acceptor−donor scaffold. The fluorescent probe, **SN4** having *N*-methylpiperazine as donors showed

significant fluorescence turn-on signaling effect in response to Aβ aggregates, including oligomers, protofibrils, and fibrils (122). The therapeutic potential can also be attended due to the incorporation of the substituted aryl piperazine scaffold that known to exhibit the anti-AD therapeutic potential and neuronal protection (113, 123). Structural analogs DPZ with potent ChEs inhibition have been reported from the past decade. Compounds containing piperazine were reported to exhibit potent inhibitory activities against AChE and BuChE, important drug targets for AD (124). The neuronal protection property is considered to be crucial for anti-AD agents. The piperazine containing compounds (**VK-28**) are known to exhibit neuronal protection (125). The designed compounds based on the above aspects were synthesized and evaluated for various spectroscopical and biological parameters.

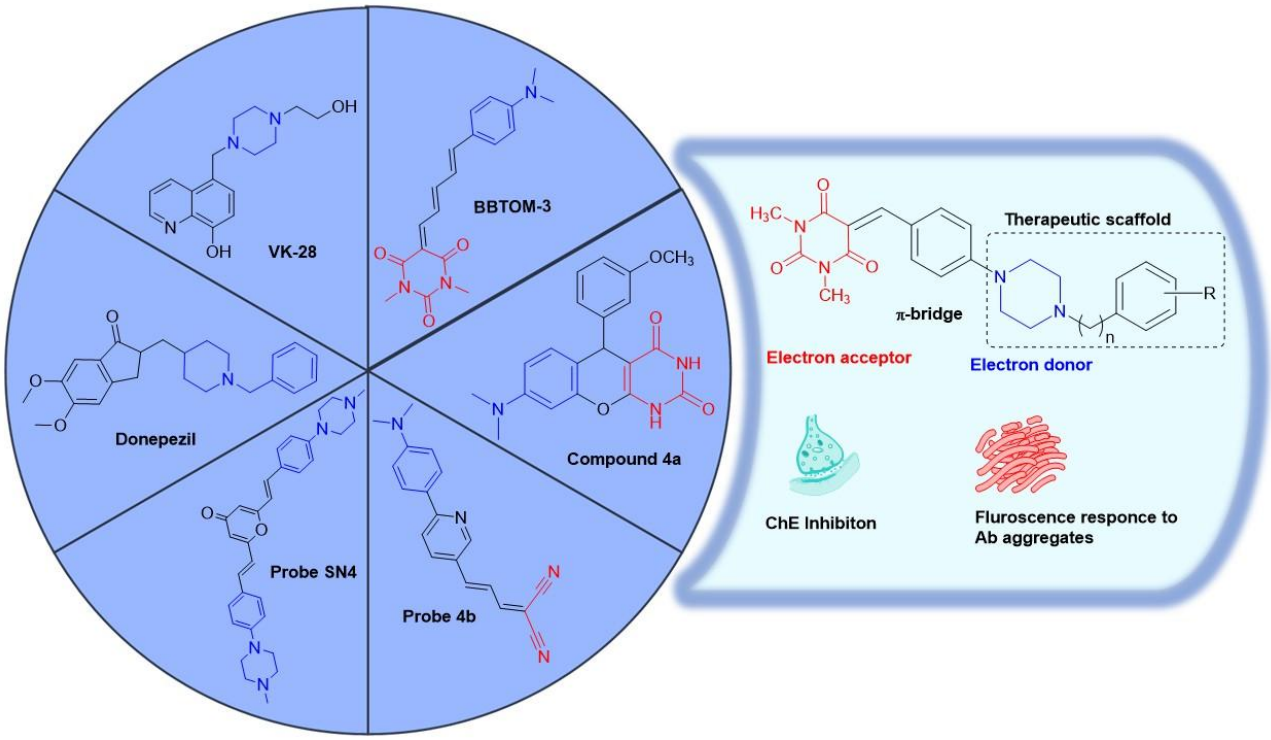

Figure 4.1. Molecular framework of design stratergy of novel theranostic fluroscent probes.

4.2 Experimental procedures

4.2.1 Chemistry

All the chemicals and reagents were purchased from different commercial suppliers viz. Alfa Acer, Avra synthesis, Sigma Aldrich and TCI Chemicals and it is directly used without any further purification unless otherwise mentioned. The precoated silica gel 60 F254 thin-layer chromatography (TLC) plates were used to monitor the progress of the reactions. Melting points of all the novel synthesized compounds were determined using an automated melting point system (Barnstead Electrothermal, UK). The proton (^{1}H) and carbon (^{13}C) NMR spectra were acquired using Bruker Advance, 500 MHz & 125 MHz spectrometers, respectively. NMR solvents, DMSO–d_6 and $CDCl_3$ were used to prepare samples at room temperature. The ppm (d values) was used to present the chemical shifts with respect to an internal standard tetramethylsilane (TMS). The % purity of all the novel synthesized compounds was determined by high-performance liquid chromatography (HPLC) with CH_3CN/H_2O/TFA (95:5:0.1%) as mobile phase in C18 column. The mass spectrum of the lead compound was obtained by using SCIEX. X500R QTOF equipped with APCI and ESI multimode ionization source instrument. The structures of all synthesized probes characterized by ^{1}H NMR, ^{13}C NMR, and HRMS are included in appendix (**Figure A.1 to A.23**).

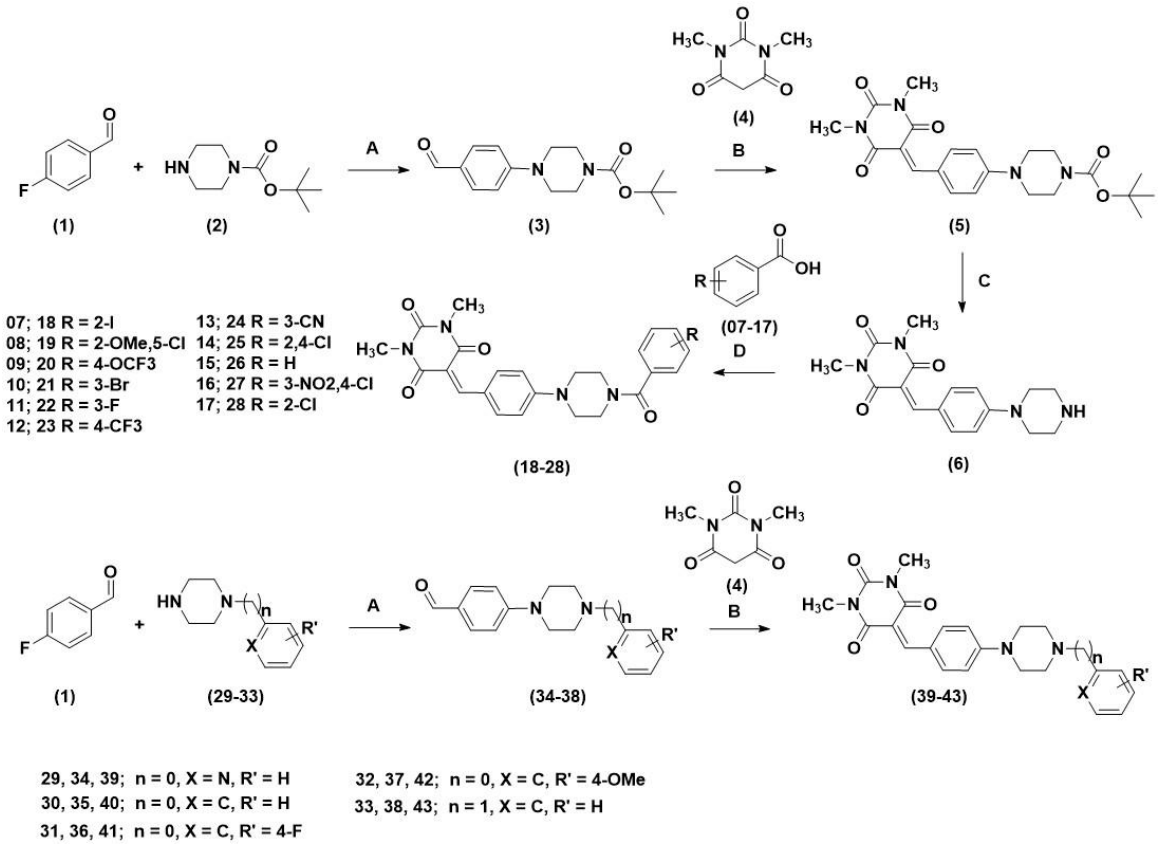

Scheme 4.1 Reagents and conditions: (**A**) 4-Fluorobenzaldehyde (**1**) 1.0 equiv, tert-Butyl piperazine-1-carboxylate (**2**) or *N*-arylpiperazine (**29-33**) 1.0 equiv, potassium carbonate 2.0 equiv, DMF,125°C, 12 h; (**B)** Intermediate (**3**)/(**34-38**) 1.0 equiv, 1,3-dimethylbarbituric acid (**5**) 1.5 equiv, Water, 70°C, 4-5h. (**C)** TFA 5.0 equiv, DCM, rt, 15-20 min; (**D)** Carboxylic acid (**07-17**) 1.2 equiv, HOBt 2.5 equiv, Diisopropylethylamine 2.5 equiv, EDCI 1.5 equiv, DCM, rt, 8 h.

4.2.1.1 General procedure for the synthesis of 3 & 34-38

To the reaction mixture of 1.0 equiv, 4-Fluorobenzaldehyde (**1**) and anhydrous potassium carbonate (K_2CO_3) (2.0 equiv) in dimethylformamide (DMF) 5 ml, appropriate substituted piperazine (**2**/**29-33**) (1.0 equiv) was added. The resultant mixture was refluxed for 12h at temperature of 120°C in a round-bottomed flask with a magnetic stirrer. TLC plate was used to monitored the progress of reaction using ethyl acetate, and hexane (4:6) as mobile phase. The resultant mixture was poured into the cold water on completion of the reaction. The formed solid crude product was filtered and washed with water and further with petroleum ether to obtain the pure product (**3**/**34-38)** in high yields.

Tert-butyl 4-(4-formylphenyl)piperazine-1-carboxylate **(3):** Bright yellow solid, yield: 81%, M.P.: 133-135 °C. ^{1}H NMR (500 MHz, $CDCl_3$): δ 9.82 (s, 1H), 7.79 (d, *J* = 8.9 Hz, 2H), 6.94 (d, *J* = 8.9 Hz, 2H), 3.64 – 3.59 (m, 4H), 3.44 – 3.38 (m, 4H), 1.51 (s, 9H). ^{13}C NMR (125 MHz, $CDCl_3$): δ 190.80, 171.09, 152.14, 129.80, 128.91, 118.58, 74.24, 61.89, 47.89, 43.99, 27.34.

4-(4-(Pyridin-2-yl)piperazin-1-yl)benzaldehyde **(34):** Dark yellow solid, yield: 77%, M.P.: 139-141 °C. ^{1}H NMR (500 MHz, $CDCl_3$): δ 9.88 (s, 1H), 8.11 (dd, J = 7.5, 1.5 Hz, 1H), 7.62 – 7.56 (m, 2H), 7.50 (td, J = 7.5, 1.5 Hz, 1H), 7.06 – 7.01 (m, 2H), 6.79 (dd, J = 7.5, 1.6 Hz, 1H), 6.66 (td, J = 7.5, 1.5 Hz, 1H), 4.09 (m, 4H), 3.36 (m, 4H). ^{13}C NMR (125 MHz, $CDCl_3$): δ 190.88, 158.86, 151.85, 148.64, 137.94, 129.80, 128.92, 118.29, 116.24, 111.31, 48.54, 46.45.

4-(4-Phenylpiperazin-1-yl)benzaldehyde **(35):** Pale yellow solid, yield: 84 %, M.P.: 141–143 °C. ^{1}H NMR (500 MHz, $CDCl_3$): δ 9.82 (s, 1H), 7.81 (d, J = 8.9 Hz, 2H), 7.05–6.95 (m, 5H), 6.90 (d, J = 9.0 Hz, 2H), 3.63–3.55 (m, 4H), 3.30–3.20 (m, 4H). ^{13}C NMR (125 MHz, $CDCl_3$): δ 190.46, 154.98, 144.65, 131.89, 130.11, 129.23, 128.54, 127.39, 118.70, 115.09, 114.59, 114.57, 113.75, 55.60, 50.64, 48.16, 47.41.

4-(4-(4-Fluorophenyl)piperazin-1-yl)benzaldehyde **(36):** Dark yellow solid, yield: 82 %, M.P.: 144–145 °C. ^{1}H NMR (500 MHz, $CDCl_3$): δ 9.88 (s, 1H), 7.59 – 7.53 (m, 2H), 7.06 – 7.03 (m, 2H), 7.03 – 6.94 (m, 4H), 3.36 (m, 4H), 3.20 (m, 4H). ^{13}C NMR (125 MHz, $CDCl_3$): δ 190.80, 160.89, 158.88, 151.85, 147.29, 147.27, 129.87, 128.87, 119.35, 119.29, 118.31, 116.46, 116.30, 49.07, 49.06, 49.04.

4-(4-(4-Methoxyphenyl)piperazin-1-yl)benzaldehyde **(37):** Pale yellow solid, yield: 83 %, M.P.: 138–140 °C. ^{1}H NMR (500 MHz, $CDCl_3$): δ 9.87 (s, 1H), 7.79 (d, J = 8.9 Hz, 2H), 7.49 (d, J = 8.2 Hz, 2H), 7.01 (d, J = 8.5 Hz, 2H) 6.68 (d, J = 8.1 Hz, 2H), 3.84–3.78 (s, 3H), 3.64–3.55 (m, 4H), 3.55–3.47 (m, 4H). ^{13}C NMR (125 MHz, $CDCl_3$): δ 191.99,

156.20, 152.81, 143.34, 135.59, 133.12, 128.59, 116.43, 115.95, 111.69, 56.04, 55.21, 50.42, 48.51, 46.35.

4-(4-Benzylpiperazin-1-yl)benzaldehyde **(38):** Dark yellow solid, yield: 82 %, M.P.: 160–162 °C. ^{1}H NMR (500 MHz, $CDCl_3$): δ 9.86 (s, 1H), 7.47 (d, J = 8.6 Hz, 2H), 7.36–7.24 (m, 4H), 7.22 (s, 1H), 6.96 (d, J = 8.1 Hz, 2H), 3.73 (s, 2H), 3.67–3.56 (m, 4H), 2.93–2.85 (m, 4H). ^{13}C NMR (125 MHz, $CDCl_3$): δ 191.99, 156.20, 138.23, 133.12, 128.58, 128.39, 127.49, 126.55, 111.79, 63.66, 56.46, 50.37, 48.72, 47.84.

4.2.1.2 General procedure for the synthesis of 5 & (39-43)

A solution of compound (**3/34-38**) (1.5 equiv) and appropriate amount of 1,3-dimethylbarbituric acid (**4**) in water was stirred at temperature of 80°C for 8−12 h. After completion of reaction, cold water was added to form the precipitate, the solution was filtered and washed with cold water. The crude product was purified by column chromatography with stationary phase silica gel (60-120 mesh) and mobile phase as mixture of ethyl acetate/n-hexane to afford desired derivatives **5; 39-43.**

Tert-butyl 4-(4-((1,3-dimethyl-2,4,6-trioxotetrahydropyrimidin-5(2H)-ylidene)methyl)phenyl)piperazine-1-carboxylate **(5):** Dark brown solid, yield: 72 %, M.P.: 178–180 °C. ^{1}H NMR (500 MHz, $CDCl_3$): δ 8.47 (s, 1H), 8.40 (d, *J* = 9.1 Hz, 2H), 6.88 (d, *J* = 9.2 Hz, 2H), 3.64 – 3.61 (m, 4H), 3.54 – 3.51 (m, 4H), 3.43 (s, 3H,), 3.42 (s, 3H), 1.51 (s, 9H). ^{13}C NMR (125 MHz, $CDCl_3$): δ 161.86, 161.81, 154.81, 151.97, 150.54, 141.21, 130.51, 127.68, 119.55, 113.50, 79.23, 47.91, 43.76, 28.35, 27.35.

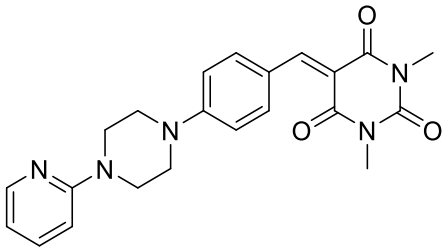

1,3-Dimethyl-5-(4-(4-(pyridin-2-yl)piperazin-1-yl)benzylidene)pyrimidine-2,4,6(1H,3H,5H)-trione **(39):** Bright red solid, yield: 78 %, M.P.: 226-228 °C. ^{1}H NMR (500 MHz, $CDCl_3$): δ 8.45 (s, 1H, ethylidene), 8.41 (d, *J* = 9.1 Hz, 2H, benzylidene C2, C6), 8.26 – 8.22 (m, 1H, pyridin-2-yl, C3), 7.58 (t, *J* = 7.1 Hz, 1H, pyridin-2-yl, C5), 6.90 (d, *J* = 9.2 Hz, 2H, benzylidene, C3, C5), 6.74 – 6.69 (m, 2H, pyridin-2-yl, C4, C6), 3.83 – 3.78 (m, 4H, piperazin-1-yl), 3.72 – 3.67 (m, 4H, piperazin-1-yl), 3.42 (s, 3H, 1,3-dimethylbarbituric acid), 3.41 (s, 3H, 1,3-dimethylbarbituric acid). ^{13}C NMR (125 MHz, $CDCl_3$): δ 163.74, 161.45, 158.54, 154.05, 151.69, 139.12, 138.32, 122.50, 113.73, 112.37, 111.24, 107.32, 46.02, 44.59, 28.98, 28.30. HRMS: *m/z* calculated for $C_{22}H_{23}N_5O_3$: 405.18 found 406.1854 [M + 1]. HPLC purity: 93.66%, retention time: 2.293 min.

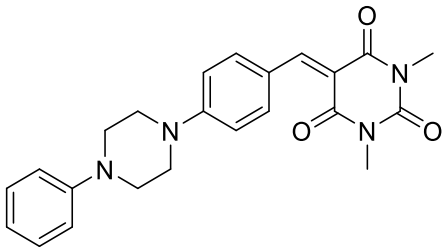

1,3-Dimethyl-5-(4-(4-phenylpiperazin-1-yl)benzylidene)pyrimidine-2,4,6(1H,3H,5H)-trione **(40):** Red solid, yield: 86 %, M.P.: 215-217 °C. ^{1}H NMR (500 MHz, $CDCl_3$): δ 8.47 (s, 1H, ethylidene), 8.42 (d, *J* = 9.2 Hz, 2H, benzylidene C2, C6), 7.35 – 7.31 (m, 2H, phenyl, C3, C5), 6.98 (d, *J* = 7.9 Hz, 2H, phenyl, C2, C6), 6.96 – 6.91 (m, 3H, phenyl C4, benzylidene, C3, C5), 3.72 – 3.67 (m, 4H, piperazin-1-yl), 3.43 (s, 3H, 1,3-dimethylbarbituric acid), 3.42 (s, 3H, 1,3-dimethylbarbituric acid), 3.39 – 3.36 (m, 4H, piperazin-1-yl).. ^{13}C NMR (125 MHz, $CDCl_3$): δ 163.76, 161.46, 158.56, 154.24, 150.67,

139.11, 129.33, 122.55, 120.42, 116.24, 112.59, 48.85, 46.56, 28.99, 28.31. HRMS: *m/z* calculated for $C_{23}H_{24}N_4O_3$: 404.18 found 405.1862 [M + 1]. HPLC purity: 99.37%, retention time: 5.233 min.

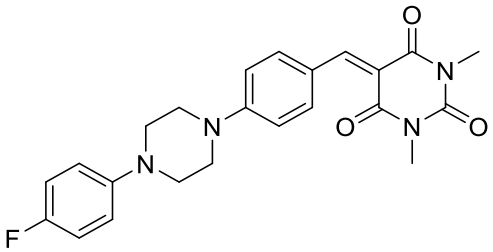

5-(4-(4-(4-Fluorophenyl)piperazin-1-yl)benzylidene)-1,3-dimethylpyrimidine-2,4,6(1H,3H,5H)-trione **(41):** Bright red solid, yield: 81 %, M.P.: 209-211 °C. ^{1}H NMR (500 MHz, $CDCl_3$): δ 8.47 (s, 1H), 8.41 (d, *J* = 9.2 Hz, 2H), 7.05 – 7.00 (m, 2H), 6.93 (dd, *J* = 9.2, 3.2 Hz, 4H), 3.70 – 3.66 (m, 4H), 3.43 (s, 3H), 3.42 (s, 3H), 3.29 – 3.26 (m, 4H). ^{13}C NMR (125 MHz, $CDCl_3$): δ 163.73, 161.44, 158.54, 156.66, 154.21, 151.69, 147.42, 147.40, 139.05, 122.64, 118.31, 118.24, 115.87, 115.70, 112.70, 49.99, 46.68, 28.99, 28.31. HRMS: *m/z* calculated for $C_{23}H_{23}FN_4O_3$: 422.18 found 423.1833 [M + 1]. HPLC purity: 96.18%, retention time: 5.193 min.

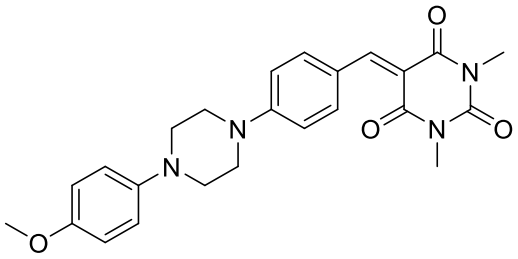

5-(4-(4-(4-Methoxyphenyl)piperazin-1-yl)benzylidene)-1,3-dimethylpyrimidine-2,4,6(1H,3H,5H)-trione **(42):** Dark orange solid, yield: 77 %, M.P.: 204-206 °C. ^{1}H NMR (500 MHz, $CDCl_3$): δ 8.47 (s, 1H, ethylidene), 8.41 (d, *J* = 8.9 Hz, 2H, benzylidene C2, C6), 7.01 – 6.86 (m, 6H, Benzylidene C3, C5, 4-methoxyphenyl C2, C6, C3, C5), 3.81 (s, 3H, 4-methoxyphenyl, CH3), 3.63 (m, 4H, piperazin-1-yl), 3.46 – 3.32 (m, 6H, 1,3-dimethylbarbituric acid), 3.29 – 3.19 (m, 4H, piperazin-1-yl). ^{13}C NMR (125 MHz, $CDCl_3$): δ 163.70, 161.41, 158.59, 156.36, 154.11, 150.66, 139.12, 139.05, 122.60,

118.72, 114.60, 112.67, 55.60, 50.57, 46.79, 28.98, 28.31. HRMS: *m/z* calculated for $C_{24}H_{26}N_4O_4$: 434.20 found 435.2116 [M + 1]. HPLC purity: 98.31%, retention time: 4.532 min.

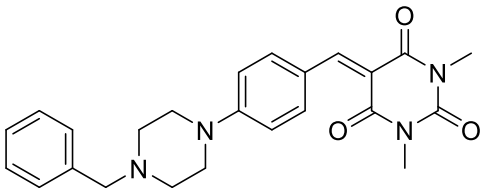

***5-(4-(4-Benzylpiperazin-1-yl)benzylidene)-1,3-dimethylpyrimidine-2,4,6(1H,3H,5H)-trione* (43):** Dark red solid, yield: 74 %, M.P.: 243-245 °C. ^{1}H NMR (500 MHz, $CDCl_3$): δ 8.36 (s, 1H), 7.62 – 7.56 (m, 2H), 7.27 (d, *J* = 2.0 Hz, 5H), 6.83 – 6.77 (m, 2H), 3.55 (s, 2H), 3.30 (s, 5H), 3.11 (t, *J* = 7.0 Hz, 4H), 2.72 (t, *J* = 7.1 Hz, 4H). ^{13}C NMR (125 MHz, $CDCl_3$): δ 160.76, 161.81, 152.16, 150.54, 141.21, 138.45, 130.51, 128.63, 128.62, 127.68, 127.25, 119.55, 113.50, 62.05, 52.58, 49.30, 27.19. HRMS: *m/z* calculated for $C_{24}H_{26}N_4O_3$: 418.20 found 418.2032 [M + 1]. HPLC purity: 93.59 %, retention time: 4.493 min.

4.2.1.3 General procedure for the synthesis of 6

A solution of compound **5** was added in dichloromethane and cooled to 0 ℃ under nitrogen environment. Drop wise addition of Trifluoroaceticacid (5.0 eq) was carried out and resulting solution was stirred at room temperature for 6 h. The completion of the reaction was monitored by TLC. The volatile solvent was evaporated under reduced pressure and obtained residue was washed with diethyl ether solvent to get the dark reddish solid compound (**6**). The solid was collected and used in the further steps.

***1,3-Dimethyl-5-(4-(piperazin-1-yl)benzylidene)pyrimidine-2,4,6(1H,3H,5H)-trione* (6):** Dark red solid, yield: 72 %, M.P.: 192-194 °C. ^{1}H NMR (500 MHz, $CDCl_3$) δ 8.66 – 8.60 (m, 2H), 8.26 (s, (s, 1H), 6.84 – 6.79 (m, 2H), 3.38 (m, 4H), 3.29 (m, 4H), 3.10 (s, 4H), 3.09 (s, 4H), 1.99 (m, 1H). ^{13}C NMR (125 MHz, $CDCl_3$): δ 162.98, 162.95, 151.86, 150.59, 141.74, 130.96, 126.58, 119.55, 113.10, 49.44, 45.99, 27.87.

4.2.1.4 General procedure for the synthesis of 18-28

To a round-bottom flask (25 ml) equipped with magnetic stirrer, 1,3-dimethyl-5-(4-(piperazin-1-yl)benzylidene)pyrimidine-2,4,6(1H,3H,5H)-trione (**6**), dichloromethane (3 ml) solvent, diisopropylethylamine (2.5 eq), respective carboxylic acid (**07-17**; 1.2 eq), and 1-Hydroxybenzotriazole (2.5 eq) were added. The mixtures were cooled to 10°C, and *N*-Ethyl-N'-(3-dimethylaminopropyl)carbodimide, Hydrochloride (1.5 eq) were added. The content was stirred at room temperature for 4-6 h. The progress of reaction was monitored by TLC, followed by the addition of water (10-15 ml). The title compounds (**18-28**) were isolated via extractive workup with ethyl acetate as solvent. The crude product was purified using column chromatography to afford desired derivatives **18-28.**

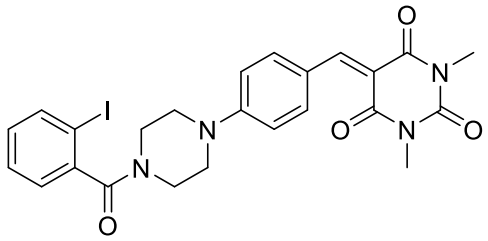

5-(4-(4-(2-Iodobenzoyl)piperazin-1-yl)benzylidene)-1,3-dimethylpyrimidine-2,4,6(1H,3H,5H)-trione **(18):** Bright red solid, yield: 81%, M.P. 241-243 °C. ^{1}H NMR (500 MHz, $CDCl_3$): δ 8.47 (s, 1H, ethylene CH), 8.38 (d, *J* = 9.1 Hz, 2H, benzylidene C_2 C6), 7.89 (d, *J* = 8.0 Hz, 1H, 2-iodobenzoyl C3), 7.46 (t, *J* = 7.5 Hz, 1H, 2-iodobenzoyl C4), 7.26 (d, *J* = 7.5 Hz, 1H, 2-iodobenzoyl C6), 7.15 (t, *J* = 7.8 Hz, 1H, 2-iodobenzoyl C5), 6.90 (d, *J* = 9.1 Hz, 2H benzylidene C3,C5), 4.10 – 4.07 (m, 1H, piperazin-1-yl), 3.95 – 3.90 (m, 1H, piperazin-1-yl), 3.72 – 3.58 (m, 3H, piperazin-1-yl), 3.52-3.46 (m, 2H, piperazin-1-yl), 3.43 (s, 3H, 1,3-dimethylbarbituric acid, CH3), 3.42 (s, 3H, 1,3-dimethylbarbituric acid, CH3), 3.38 – 3.31 (m, 1H, piperazin-1-yl). ^{13}C NMR (125 MHz, $CDCl_3$): δ 169.50, 158.49, 153.76, 151.62, 139.40, 138.76, 130.63, 129.76, 128.62, 127.12, 120.03, 113.05, 92.47, 46.11, 41.14, 29.02, 28.34. HRMS: *m/z* calculated for

$C_{24}H_{23}IN_4O_4$: 558.08 found 559.1610 [M + 1]. HPLC purity: 84.46%, retention time: 4.720 min.

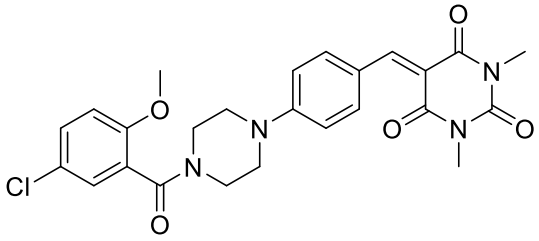

5-(4-(4-(5-Chloro-2-methoxybenzoyl)piperazin-1-yl)benzylidene)-1,3-dimethylpyrimidine-2,4,6(1H,3H,5H)-trione **(19):** Dark red solid, yield: 84%, M.P. 234-236 °C. ^{1}H NMR (500 MHz, $CDCl_3$): δ 8.47 (s, 1H, ethylene CH), 8.38 (d, *J* = 9.0 Hz, 2H, benzylidene C_2 C6), 7.38 (d, *J* = 8.8, 2.6 Hz, 1H, 5-chloro-2-methoxybenzoyl C4), 7.28 (s, 1H, 5-chloro-2-methoxybenzoyl C6), 6.95 (d, *J* = 9.1 Hz, 2H, benzylidene C3,C5), 6.91 (d, *J* = 8.9 Hz, 1H, 5-chloro-2-methoxybenzoyl C4), 4.02 – 3.97 (m, 2H, piperazin-1-yl), 3.86 (s, 3H, 2-methoxy(benzoyl) CH3), 3.62 (t, *J* = 4.6 Hz, 2H, piperazin-1-yl), 3.47 (t, *J* = 11.5 Hz, 4H, piperazin-1-yl), 3.43 (s, 3H, 1,3-dimethylbarbituric acid, CH3), 3.41 (s, 3H, 1,3-dimethylbarbituric acid, CH3). ^{13}C NMR (125 MHz, $CDCl_3$): δ 166.43, 163.51, 161.31, 158.36, 153.94, 151.59, 138.60, 130.62, 128.19, 126.46, 126.30, 123.62, 113.34, 112.41, 56.01, 47.53, 46.86, 45.88, 41.16, 29.02, 28.34. HRMS: *m/z* calculated for $C_{25}H_{25}ClN_4O_5$: 496.15 found 497.1810 [M + 1]. HPLC purity: 98.98 %, retention time: 4.527 min.

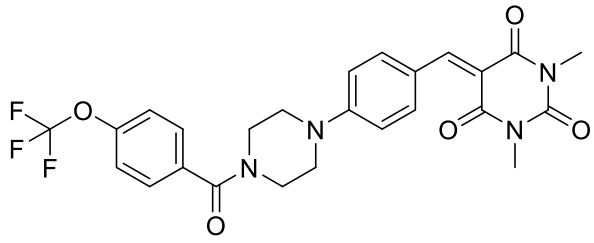

1,3-Dimethyl-5-(4-(4-(4-(trifluoromethoxy)benzoyl)piperazin-1-yl)benzylidene)pyrimidine-2,4,6(1H,3H,5H)-trione **(20):** Bright red solid, yield: 79%, M.P. 242-244 °C. ^{1}H NMR (500 MHz, $CDCl_3$): δ 8.46 (s, 1H, ethylene), 8.39 (d, *J* = 9.1 Hz, 2H, benzylidene C2, C6), 7.52 (d, *J* = 8.6 Hz, 2H, 4-(4-(trifluoromethoxy)benzoyl),

C2, C6), 7.31 (d, *J* = 8.1 Hz, 2H, 4-(4-(trifluoromethoxy)benzoyl), C3, C5), 6.90 (d, *J* = 9.1 Hz, 2H, benzylidene C3 C5), 4.01 – 3.83 (m, 2H, piperazine, C3 C5), 3.71 – 3.48 (b, 6H, piperazine, C3 C5 C2 C6), 3.42 (s, 3H, 1,3-dimethylbarbituric acid, CH3), 3.41 (s, 3H, 1,3-dimethylbarbituric acid, CH3). ^{13}C NMR (125 MHz, CDCl3): δ 169.45, 163.58, 161.36, 158.47, 153.80, 151.60, 150.42, 138.74, 133.46, 129.07, 123.22, 121.05, 113.00, 112.17, 46.91, 46.82, 29.02, 28.34. HRMS: *m/z* calculated for $C_{25}H_{23}F_3N_4O_5$: 516.16 found 517.1637 [M + 1]. HPLC purity: 85.57%, retention time: 4.673 min.

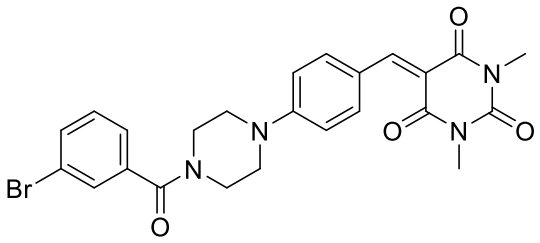

5-(4-(4-(3-Bromobenzoyl)piperazin-1-yl)benzylidene)-1,3-dimethylpyrimidine-2,4,6(1H,3H,5H)-trione **(21):** Bright red solid, yield: 84%, M.P.238-240 °C. ^{1}H NMR (500 MHz, $CDCl_3$): δ 8.46 (s, 1H, ethylene), 8.37 (d, *J* = 8.8 Hz, 2H, benzylidene C2, C6), 7.62 – 7.61 (m broad, 2H, 3-bromobenzoyl C2, C6), 7.39 (d, *J* = 7.5 Hz, 1H, 3-bromobenzoyl C4), 7.34 (t, *J* = 7.9 Hz, 1H, 3-bromobenzoyl C5), 6.91 (d, *J* = 8.9 Hz, 2H, benzylidene C3, C5), 3.96 (d, *J* = 6.0 Hz, 2H, piperazin-1-yl), 3.65 – 3.51 (m, 6H, piperazin-1-yl), 3.42 (s, 3H, 1,3-dimethylbarbituric acid, CH3), 3.40 (s, 3H, 1,3-dimethylbarbituric acid, CH3). ^{13}C NMR (125 MHz, CDCl3): δ 168.85, 163.49, 161.29, 158.35, 153.51, 151.57, 138.60, 137.02, 133.28, 130.32, 125.70, 123.57, 122.85, 113.26, 47.00, 41.76, 29.01, 28.33. HRMS: *m/z* calculated for $C_{24}H_{23}BrN_4O_4$: 510.09 found 511.1666 [M + 1]. HPLC purity: 99.29 %, retention time: 4.773 min.

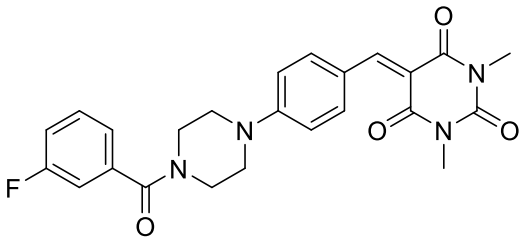

5-(4-(4-(3-Fluorobenzoyl)piperazin-1-yl)benzylidene)-1,3-dimethylpyrimidine-2,4,6(1H,3H,5H)-trione **(22):** Dark brown solid, yield: 74%, M.P. 207-209 °C. ^{1}H NMR (500 MHz, $CDCl_3$): δ 8.46 (s, 1H, ethylene), 8.37 (d, *J* = 9.0 Hz, 2H, benzylidene, C2, C6), 7.47 – 7.41 (m, 1H, 3-fluorobenzoyl C5), 7.24 (d, *J* = 7.6 Hz, 1H, 3-fluorobenzoyl C6), 7.21 – 7.16 (m, 2H, 3-fluorobenzoyl, C4, C2)., 6.91 (d, *J* = 9.1 Hz, 2H, benzylidene C3 C5), 3.95 (d, *J* = 3.9 Hz, 2H, piperazin-1-yl), 3.73 – 3.45 (m, 6H, piperazin-1-yl), 3.42 (s, 3H, 1,3-dimethylbarbituric acid, CH3), 3.40 (s, 3H, 1,3-dimethylbarbituric acid, CH3). ^{13}C NMR (125 MHz, $CDCl_3$): δ 169.11, 163.52, 161.63, 161.32, 158.38, 153.60, 151.59, 138.64, 137.15, 130.60, 123.49, 122.84, 122.82, 117.38, 117.21, 114.63, 114.45, 113.21, 112.36, 47.00, 41.87, 29.01, 28.33. HRMS: *m/z* calculated for $C_{24}H_{23}FN_4O_4$: 450.17 found 451.2410 [M + 1]. HPLC purity: 98.06%, retention time: 4.333 min.

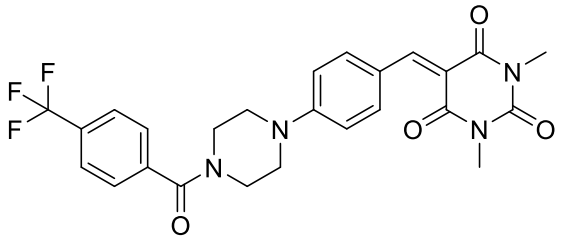

1,3-Dimethyl-5-(4-(4-(4-(trifluoromethyl)benzoyl)piperazin-1-yl)benzylidene)pyrimidine-2,4,6(1H,3H,5H)-trione **(23):** Brown-red solid, yield: 85%, M.P. 208-210 °C. ^{1}H NMR (500 MHz, $CDCl_3$): δ 8.48 (s, 1H, ethylidene), 8.38 (d, *J* = 9.0 Hz, 2H, benzylidene C2, C6), 7.75 (d, *J* = 8.0 Hz, 2H, 5-(trifluoromethyl)benzoyl C2, C6), 7.60 (d, *J* = 7.9 Hz, 2H, 5-(trifluoromethyl)benzoyl C3, C5), 6.92 (d, *J* = 9.1 Hz, 2H, benzylidene C3, C5), 3.99 (s, 2H piperazine, C3, C5), 3.64 (s, 4H, piperazin-1-yl), 3.51 (s, 2H, piperazin-1-yl), 3.43 (s, 3H, 1,3-dimethylbarbituric acid, CH3), 3.41 (s, 3H, 1,3-dimethylbarbituric acid, CH3). ^{13}C NMR (125 MHz, $CDCl_3$): δ 169.12, 163.51, 161.32, 158.42, 153.60, 151.58, 138.61, 127.57, 125.84, 125.81, 123.53, 114.44, 113.21, 112.45, 47.20, 40.94, 29.02, 28.34. HRMS: *m/z* calculated for $C_{25}H_{23}F_3N_4O_4$: 500.17 found 501.1910 [M + 1]. HPLC purity: 99.59 %, retention time: 4.727 min.

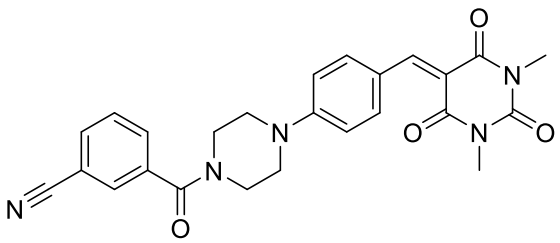

3-(4-(4-((1,3-Dimethyl-2,4,6-trioxotetrahydropyrimidin-5(2H)-ylidene)methyl)phenyl)piperazine-1-carbonyl)benzonitrile **(24):** Dark red solid, yield: 82%, M.P. 218-220 °C. ^{1}H NMR (500 MHz, $CDCl_3$): δ 8.47 (s, 1H, ethylidene), 8.38 (d, J = 9.1 Hz, 2H, benzylidene C2, C6), 7.79 (d, J = 9.1 Hz, 2H, benzonitrile, C4 C6), 7.72 (d, J = 7.9 Hz, 1H, , benzonitrile C2), 7.61 (t, J = 7.7 Hz, 1H, benzonitrile, C5), 6.90 (d, J = 9.2 Hz, 2H, benzylidene C3, C5), 3.96 (s, 2H, piperazin-1-yl), 3.57 (bs, , 6H, piperazin-1-yl), 3.42 (s, 3H, 1,3-dimethylbarbituric acid, CH3), 3.41 (s, 3H, 1,3-dimethylbarbituric acid, CH3). ^{13}C NMR (125 MHz, $CDCl_3$): δ 168.13, 163.52, 161.33, 158.44, 153.71, 151.58, 138.67, 136.44, 133.63, 131.48, 130.85, 129.75, 123.37, 117.82, 113.10, 112.38, 47.04, 42.05, 29.02, 28.34. HRMS: *m/z* calculated for $C_{25}H_{23}N_5O_4$: 457.18 found 458.1822 [M + 1]. HPLC purity: 91.62%, retention time: 4.427 min.

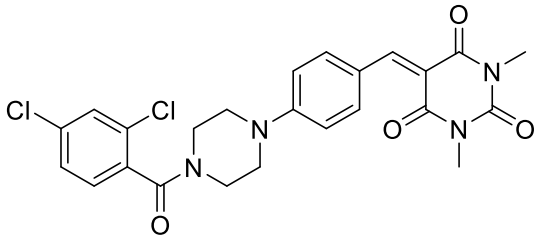

5-(4-(4-(2,4-Dichlorobenzoyl)piperazin-1-yl)benzylidene)-1,3-dimethylpyrimidine-2,4,6(1H,3H,5H)-trione **(25):** Bright red solid, yield: 77%, M.P.220-222 °C. ^{1}H NMR (500 MHz, $CDCl_3$): δ 8.46 (s, 1H, ethylidene)), 8.37 (d, *J* = 9.1 Hz, 2H, benzylidene C2, C6), 7.49 (d, *J* = 1.9 Hz, 1H, 2,4-dichlorobenzoyl, C6), 7.37 (d, *J* = 8.2, 1.9 Hz, 1H, 2,4-dichlorobenzoyl, C5), 7.30 (s, 1H, 2,4-dichlorobenzoyl, C3), 6.89 (d, *J* = 9.2 Hz, 2H, benzylidene C3, C5), 4.09 – 3.87 (m, 2H, piperazin-1-yl), 3.63 (bs, 2H, piperazin-1-yl), 3.50 (t, *J* = 19.5 Hz, 4H, piperazin-1-yl), 3.42 (s, 3H, 1,3-dimethylbarbituric acid, CH3), 3.41 (s, 3H, 1,3-dimethylbarbituric acid, CH3). ^{13}C NMR (125 MHz, $CDCl_3$): δ 166.15,

163.54, 161.34, 158.44, 153.74, 151.59, 138.71, 136.05, 133.69, 131.31, 129.76, 128.87, 127.90, 123.25, 113.08, 112.24, 47.06, 46.47, 45.95, 41.29, 29.02, 28.33. HRMS: *m/z* calculated for $C_{24}H_{22}Cl_2N_4O_4$: 500.10 found 501.1042 [M + 1]. HPLC purity: 99.76%, retention time: 4.940 min.

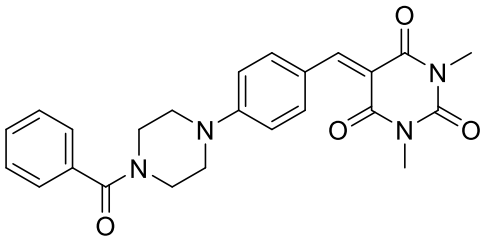

***5-(4-(4-Benzoylpiperazin-1-yl)benzylidene)-1,3-dimethylpyrimidine-2,4,6(1H,3H,5H)-trione* (26):** Bright red solid, yield: 84%, M.P. 241-243 °C. ^{1}H NMR (500 MHz, $CDCl_3$): δ 8.47 (s, 1H, ethylidene), 8.39 (d, *J* = 9.1 Hz, 2H, benzylidene C2, C6), 7.47 (bs, 5H, benzoyl, C2,C6, C4, C3, C5), 6.89 (d, *J* = 9.2 Hz, 2H, benzylidene C3, C5), 3.96 (d, *J* = 8.9 Hz, 2H, piperazin-1-yl), 3.77 – 3.46 (m, 6H, piperazin-1-yl), 3.43 (s, 3H, 1,3-dimethylbarbituric acid, CH3), 3.41 (s, 3H, 1,3-dimethylbarbituric acid, CH3). ^{13}C NMR (125 MHz, $CDCl_3$): δ 170.67, 163.62, 161.39, 158.53, 153.95, 151.65, 138.82, 135.10, 130.23, 128.71, 127.19, 123.10, 112.95, 112.03, 47.59, 46.10, 29.01, 28.33. HRMS: *m/z* calculated for $C_{24}H_{24}N_4O_4$: 432.18 found 433.2131 [M + 1]. HPLC purity: 96.56%, retention time: 4.387min.

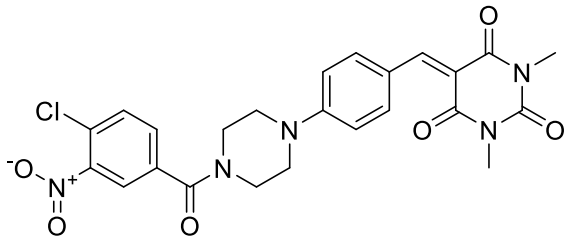

***5-(4-(4-(4-Chloro-3-nitrobenzoyl)piperazin-1-yl)benzylidene)-1,3-dimethylpyrimidine-2,4,6(1H,3H,5H)-trione* (27)**: Dark brown solid, yield: 78%, M.P. 238-240 °C. ^{1}H NMR (500 MHz, $CDCl_3$): δ 8.47 (s, 1H, ethylidene), 8.37 (d, *J* = 8.9 Hz, 2H, benzylidene C2, C6), 8.01 (s, 1H, 4-chloro-3-nitrobenzoyl, C2), 7.67 (q, *J* = 8.2 Hz, 2H, 4-chloro-3-nitrobenzoyl C6, C5), 6.94 (d, *J* = 9.0 Hz, 2H, benzylidene C3, C5), 3.97 (s, 2H,

piperazin-1-yl), 3.80 – 3.48 (m, 6H, , piperazin-1-yl), 3.43 (s, 3H, 1,3-dimethylbarbituric acid, CH3), 3.41 (s, 3H, 1,3-dimethylbarbituric acid, CH3). ^{13}C NMR (125 MHz, $CDCl_3$): δ 166.94, 163.43, 161.27, 158.33, 153.25, 151.55, 147.88, 138.46, 134.75, 132.51, 131.86, 129.12, 124.71, 123.90, 113.44, 112.77, 47.19, 46.80, 29.04, 28.35. HRMS: *m/z* calculated for $C_{24}H_{22}ClN_5O_6$: 511.13 found 512.1316 [M + 1]. HPLC purity: 92.31%, retention time: 4.307 min.

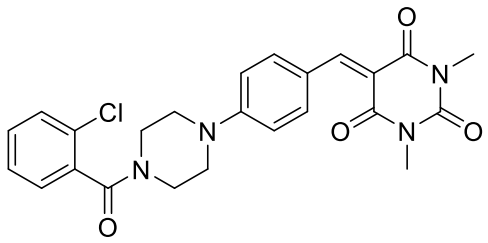

5-(4-(4-(2-Chlorobenzoyl)piperazin-1-yl)benzylidene)-1,3-dimethylpyrimidine-2,4,6(1H,3H,5H)-trione **(28):** Red solid, yield: 80%, M.P. 246-248 °C: ^{1}H NMR (500 MHz, $CDCl_3$): δ 8.46 (s, 1H, ethylidene), 8.37 (d, *J* = 9.1 Hz, 2H, benzylidene C2, C6), 7.46 (d, *J* = 1.9 Hz, 1H, 2-chlorobenzoyl, C5), 7.42 – 7.32 (m, 3H, 2-chlorobenzoyl, C2, C3, C4), 6.91 (d, *J* = 9.2 Hz, 2H, benzylidene C3, C5), 4.10 (s, 1H, piperazin-1-yl), 3.93 (s, 1H, piperazin-1-yl), 3.64 (d, *J* = 4.3 Hz, 2H, piperazin-1-yl), 3.51 (dd, *J* = 22.8, 15.5 Hz, 4H, piperazin-1-yl), 3.42 (s, 3H, 1,3-dimethylbarbituric acid, CH3), 3.41 (s, 3H, 1,3-dimethylbarbituric acid, CH3). ^{13}C NMR (125 MHz, $CDCl_3$): δ 167.07, 163.54, 161.32, 158.41, 153.63, 151.60, 138.70, 135.22, 130.63, 130.34, 129.82, 127.90, 127.45, 123.36, 113.17, 112.23, 47.20, 46.63, 45.88, 41.15, 29.01, 28.33. HRMS: *m/z* calculated for $C_{24}H_{23}ClN_4O_4$: 466.14 found 467.1622 [M + 1]. HPLC purity: 97.42%, retention time: 4.487 min.

4.2.2 *In-vitro* cholinesterase inhibition

The *in vitro* cholinesterase inhibitory potential of the synthesized compounds was evaluated spectrometrically as per the previously reported protocol of modified Ellman colorimetric assay (126). The cholinesterase enzymes, *ee*AChE and *eq*BuChE were

purchased from Sigma Aldrich (USA). In brief, the stock solutions of test compounds (**18-28** & **39-43**) were prepared in biological grade DMSO and further working concentrations were prepared in PBS solution to determine the IC_{50}. It involved the breakdown of thiolated substrates catalyzed by the cholinesterase to produce thiocholine which reduced 5,5-dithio-bis-(2- nitrobenzoic acid (DTNB) to produce yellow coloured product that can be detected colorimetrically. The assay procedure involved the incubation of test compounds / standard compound (10 ul) with the 50 µl of *ee*AChE (0.22 U/ml) or 50 µl of *eq*BuChE (0.06 U/ml) enzyme in 96-well plates for 30 min at room temperature. Further, ATCI (15 mM) or BTCI (15 mM) substrate (30 µl) was added and incubated for another 30 min. Then, 160 µl solution of DTNB solution (1.5 mM) was added to each well, and absorbance was measured at 412 nm using Synergy HTX multi-mode reader (BioTek, USA). The blank control contained all the components except the enzyme. The donepezil was used as a positive control in the study. The assay was independently repeated two to three times in triplicate. The percentage inhibitory potential for test compounds was calculated.

4.2.3 *In-vitro* blood-brain barrier permeation assay

The *in vitro* blood-brain barrier permeability of the test compounds was assessed by PAMPA model using previously reported protocol with minor modifications. Concisely, 5 µl of porcine brain lipid (20 mg/ml in dodecane) was used to coat the bottom porous filter disks of acceptor plates and incubated overnight to get saturated. The biological grade DMSO was used to make the stock solutions of test compound (10 mM) and further dilution, 500 µM (500 µl) made using PBS. The equilibrium standard of each test compound (200 µl) was prepared by adding 120 µl of PBS in 80 µl of 500 µM of test compound. Finally, blank control (250 µl) was prepared with 5 µl of DMSO in 245 µl PBS. The equilibrium standard and blank control were set aside for analysis on the next

day. Initially, the PBS of 300 µl was added in the acceptor plate. Then, 200 µl of each test compound (500 µM) and permeability controls were added in the wells of the donor plate (0.45 mm pore size of membrane) in duplicate. To ease the diffusion of test compound into the acceptor well from the donor part through lipid membrane, the donor plate was kept carefully into the acceptor plate wells like a sandwich and incubated for the period of 18 h at 37°C. The donor plates were removed after the incubation period, and absorbance of the drug in the acceptor well and equilibrium standard were measured. The absorbance spectrum from wavelength 200 nm to 500 nm was recorded using a microplate reader. The experiments were performed in duplicate. The Pe values were calculated using the following expression; Pe = C × -In (1- ODA/ ODE) cm/s, where, ODA & ODE are the absorbance of acceptor and equilibrium standard, respectively, and value of C was taken as 7.72×10^{-6}, based on the experiments were running for the period of 18 hrs. The results are represented as the mean ± SD.

4.2.4 Measurement of photophysical properties

The fluorescence data, including the excitation and emission wavelengths of all the synthesized probes were measured in PBS (10% DMSO). The solvatochromism properties of lead probe **39** was performed to evaluate the exact spectral characteristics, the absorption, excitation, and emission spectra in different solvent.

4.2.5 Binding studies with $A\beta_{1-42}$ aggregates

$A\beta_{1-42}$ peptide was purchased from Cayman chemical. Firstly, the stock solution of $A\beta_{1-42}$ was made by dissolving lyophilized aliquot of $A\beta_{1-42}$ in 1 % NH_4OH and sterile PBS (pH 7.4) and was stored at temperature of - 80 ◦C. The required dilutions were prepared with PBS to make a working solution of $A\beta_{1-42}$ peptide. The $A\beta_{1-42}$ monomers were incubated for 72h to prepare aggregated $A\beta_{1-42}$ peptide and the aggregation degree of $A\beta_{1-42}$ peptide was determined by ThT fluorescence assay. The fluorescent properties of free

probe **39** in the aqueous solution to their fluorescence properties in the presence of $A\beta_{1-42}$ aggregates was determined. The probe **39**: $A\beta_{1-42}$ peptide was taken in a ratio of 2:1 in the final solution mixture. To the solutions of test probes (30 μL, 50 μM) in PBS (pH = 7.4) was added $A\beta_{1-42}$ (30 μL, 25 μM) peptide suspension in PBS (pH = 7.4). To evaluate the change in the fluorescence response probe **39** (50 μM) was incubated for 15 min with aggregated $A\beta_{1-42}$ proteins. The resulted mixture was transferred to a 384-well plate black (n = 3), and the plate was subjected to fluorescence imaging using (BioTek Synergy H1M) fluorescence spectrophotometer.

4.2.6 *In vitro* saturation binding assay using $A\beta_{1-42}$ aggregates

A solution of $A\beta_{1-42}$ aggregates (final concentration of 50 μM) was mixed with different concentrations of probe **39** (0, 20, 40, 60, 80, 100 and 200 μM) and incubated at room temperature for 5 min. Fluorescence intensities of the resultant mixture were measured by a fluorescence spectrometer at 650 nm. The K_d binding curve was generated by software prism with nonlinear one-site binding regression.

4.2.7 *In situ* fluorescence imaging of Aβ aggregation

A solution of Aβ aggregates was incubated for the 10 min with Probe **39** in a ratio of 2:1 in the final solution mixture. The sample was spin coated on a quartz coverslip for fluorescence microscopy imaging. The imaging experiment was performed in a homebuilt widefield epifluorescence microscopy setup. A continuous wave DPPS laser (405 nm for ThT and 488 nm for probe **39**) was reflected upwards by a dichroic mirror (DM) to hit the prepared sample on quartz coverslip via oil objective lens (1.49NA, 60x, Nikon, Apo TIRF). The fluorescence emitted from the sample was collected by the same objective lens and then passed through the same DM and a bandpass filter (435-485 nm for ThT and 590-700 nm for probe **39**). The filtered emission was recorded by an air-cooled s-CMOS (ORCA-flash 4.0 V3, Hamamatsu) at a rate of 5 frames per second (fps).

The excitation laser power of 405 nm and 488 nm was kept at 7 µW and 60 µW, respectively after the objective lens for every photoluminescence (PL) measurements and was measured using a power meter (laser check, coherent). All the microscopic images were analyzed by using ImageJ (NIH) and OriginPro 2021 (OriginLab, USA) software.

4.2.8 Fluorescence lifetime measurement

TCSPC spectrometer was used for recording the PL decay at magic angle (54.7˚) polarization (λ_{ex} = 440nm). Details of the setup can be found else here (127). EzTime software was used to analyze the PL decay. Iterative Deconvolution method was used to calculate the time constants of PL decay using the following equation.

$$I(t) = I_0(\lambda)\, \Sigma_i a_i\, e^{-t/\tau_i} \quad \ldots\ldots \textbf{(i)}$$

Micro Time 200 (Pico Quant, GmbH, Germany) instrument equipped with an epifluorescence microscope (Olympus 1X-71) and two single avalanche photodiodes (SPAD's) was used for the fluorescence lifetime imaging. Where, 440 nm pulsed diode laser (PDL828 S Sepia II, Pico quant) of 10 MHz repetition rate was used for the excitation. Measurement was done in time tagged time resolved (TTTR) mode. A 590-700 nm (Chroma) band pass filter was used to block the excitation laser in the path and the signal was recorded using single avalanche photodiodes. All the analysis for FILM data was done in SymphoTime 64 (PicoQuant) and OriginPro 2021 (OriginLab, USA) software.

4.2.9 Density Functional Theory (DFT) calculation

The energy minimized structures were obtained from the DFT with Becke 3-parameter exchange functional and the gradient-corrected correlation functional of Lee, Yang, and Parr (B3LYP) by the B3LYP/6-311G (d,p) basis set. All these calculations were performed with Gaussian 09 (128, 129, 130).

4.2.10 Molecular docking

The molecular docking studies of the selected structures into the active sites of both AChE (**4EY7**) (131) and $A\beta_{1-42}$ species (**5OQV**) (32) proteins were performed on Autodock 4 software by employing Lamarckian Genetic Algorithm (LGA). The Discovery Studio 2021 client version used for the preparation of protein structures and ligands structures were drawn on the Chem 3D. The grid parameters were fixed by considering amino acids from the active sites of both respective targets of AChE and $A\beta_{1-42}$ species. The genetic algorithms selected were set to 100 runs. The parameters for docking were marked as default, followed by employing Lamarckian Genetic Algorithm (LGA) and further generated the both grid and docking parameter files, i.e., gpf and dpf, respectively. Finally, the interaction of ligand-protein was visualized by using Discovery studio visualizer software (132).

4.2.11 *In vivo* Biological evaluations

4.2.11.1 Animals, housing, and ethical approval

The Swiss albino mice of either sex were procured and acclimatized for the period of 7 days in the ambient conditions with temperature (25 ± 2 °C), relative humidity (65 ± 5%) and 12:12 h dark/light cycle at the institute animal house facility, Department of Pharmaceutical Engineering & Technology, IIT (BHU), Varanasi. All the experimental protocols were executed following the CPSCEA guidelines that duly permitted by the Institutional Animal Ethical Committee (IAEC), IIT (BHU), Varanasi with IAEC approval number: IIT(BHU)/IAEC/2024/I/034.

4.2.11.2 Acute toxicity studies

The most promising compound **39** was evaluated for acute oral toxicity testing as per the OECD 423 guidelines using female albino mice. As per protocol, the experimental animals were divided into two different groups (n = 3), control group was administered

orally with vehicle alone, and second group administered with single dose of compound **39** (300 mg/kg, po). For up to next 14 days, all the animals were observed for toxic symptoms, change in body weight, food consumption, behavioural changes, toxic reactions, and mortality. Animals were sacrificed, and isolated the organs, i.e., brain, liver, kidney, and heart after 14 days. The transverse sections (15 μm) of tissues were made using a cryostat, mounted on the glass slide, then stained with dyes hematoxylin and eosin, and observed under the microscope (Magnus MLX plus India at 10x resolution).

4.2.11.3 Behavioural studies

4.2.11.3.1 Drugs and chemicals

Scopolamine HCl and Donepezil HCl were purchased from the sigma-aldrich, India. ACh ELISA kit was acquired from the krishgen bio systems, India. For the estimation of MDA and CAT levels, the ELISA kits were purchased from ELK Biotechnology. All the other reagents used in the studies were purchased from the different commercial suppliers.

4.2.11.3.2 Drug preparation and treatment protocols

The scopolamine (3 mg/kg) and DPZ in the dose of 5 mg/kg were used and the solution of compound **39** (5, 10, and 20 mg/kg) was freshly prepared in the suspension of 0.3% sodium carboxy methyl cellulose. The experimental animals were divided into six different groups based on the random selection (n = 6), including (i) Control group, (ii) Scopolamine (3 mg/kg, i.p.) group, (iii) Compound **39** (5 mg/kg, p.o.) group, (iv) Compound **39** (10 mg/kg, p.o.) group, and (v) Compound **39** (20 mg/kg p.o.) group (vi) DPZ (5 mg/kg, p.o.) group. Test compound **39** and reference standard DPZ were administered daily for up to 7 days. On the seventh day of experiment, the scopolamine (3 mg/kg, i.p.) was given to all animal group excluding the control group after 30 minutes of drug administration. Only solution of vehicles was administered to the control group.

All the animals were put through the Y-maze test after 15 minutes of the administration of vehicle or scopolamine.

4.2.11.3.3 Y-maze test

The spatial working and exploratory behavior in rodents can be assess with widely used simple, quick, and sensitive test i.e., Y-maze test (133). Three-dimensional (3D) horizontal maze set apart by the 120° was used to examined the spontaneous alternation behavior and number of entries. Three different arms were named as A, B, and C. In the testing, each mouse was placed individually at the center of the maze and allowed for free movement and recorded for up to 8 minutes. The video camera was used to record the entry of each mouse into each arm. Further, the obtained data was analyzed, and calculated the percentage of alternation. The spontaneous alternation was considered when the mice entered the three different arms (ABC, ACB, BAC, BCA, CAB, and CBA). The following formula were used to determined percentage alternation: % spontaneous alternation (SA) = [number of spontaneous alternations/ (total arm entries – 2)] X 100. The % SA shows the short-term memory in mice.

4.2.11.4 *Ex-vivo* biochemical analysis

The experimental mice from each respective group were sacrificed after *in vivo* behavioural experiment through the cervical dislocation method. The brains were separated from the skull and the regions of hippocampus and cortex were carefully isolated, then homogenized with a glass homogenizer in 12.5 mM of 5 ml PBS buffer and centrifuged 30 min at 7000 rpm at 4°C to obtained supernatants. The collected supernatants were used for the estimation of different biochemical parameters. The supernatants were examined for the levels of ACh using the ACh ELISA kit. The cholinergic marker, AChE levels was estimated by the modified Ellman's colorimetric assay method (113, 134). In brief, the isolated supernatant (50 µl) was initially incubated

with the 15 mM of freshly prepared ATCI (30 µl) for 30 min, then the 160 µl of DTNB (1.5 mM) were added and the absorbance was determined immediately at λ = 415 nm. Further, brain supernatant was used to estimate the levels of CAT and MDA. The assay to estimate MDA and CAT levels were performed using ELISA kits from ELK Biotechnology, following the manufacturer's guidelines/protocol.

4.3 Results and discussion

4.3.1 Chemistry

The designed probes were synthesized as mentioned in **Scheme 4.1** yielding compounds/probes **18-28** & **39-43**. The reaction of 4-fluorobenzaldehye (**1**) with tert-Butyl piperazine-1-carboxylate (**2**) or *N*-arylpiperazine (**29-33**) along with strong base potassium carbonate (K_2CO_3) underwent nucleophilic substitution reaction (126) to afford first intermediates (**3**) and **34-38,** respectively. Then the second intermediates (**5**) or target probes (**39-43**) were synthesized by the reacting the obtained intermediate containing free aldehyde group with 1,3-dimethylbarbituric acid (**4**). The present reaction is Knoevenagel condensation of aldehyde derivatives (**3** & **34-38**) on the active methylene of 1, 3-dimethylbarbituric acid (**4)** in water resulting in the formation of second intermediates (**6**) and target probes (**39-43**). The key intermediate **(6**) was obtained in good yield on the removal of Boc protecting group with trifluoroacetic acid (TFA). Finally, target probes (**18-28)** were synthesized by reacting the key intermediate (**6**) with various carboxylic acids (**7-17**). The amide derivatives (**18-28**) were prepared by using *N*-Ethyl-*N*′-(3-dimethylaminopropyl) carbodiimide hydrochloride (EDCI) and 1-hydroxybenzotriazolehydrate (HOBt) as a catalyst in dichloromethane solvent. The structures of all synthesized probes are represented in **Table 4.1** as characterized by ^{1}H NMR, ^{13}C NMR, and HRMS in appendix. The % purity of all the probes were assessed by HPLC analysis and were found to be highly pure.

4.3.2 *In-vitro* cholinesterase inhibition

The cholinergic neurotransmission in AD can be enhanced through cholinesterase inhibitors. Therefore, concurrent targeting of both AChE and BuChE would be appealing approach for development of anti-AD agents (113). Accordingly, all the synthesized compounds (**18-28 & 39-43**) were analyzed for their both ChEs inhibitory potential using donepezil and rivastigmine as positive reference standards. In this study, the enzymes from the animal sources (AChE from electric eel, *ee*AChE, and BuChE from equine serum, *eq*BuChE) were utilized due to their higher degree of sequence homology and lower cost as compared to human enzymes. The results showed excellent inhibition of AChE in micromolar concentration range as shown in **Table 4.1.** All the tested compounds elicited poor inhibitory potential against BuChE except compound **43** of the series bearing *N*-benzyl piperazine moiety. Among all the tested compounds, compound **39** & **43** have pronounced AChE inhibitory activity. The compounds containing carbonyl group as a linker between piperazine and aryl moieties (**18-28**) showed good to moderate inhibitory profiles. Among compounds **18-28**, the bromo substituted carbonyl containing compound **21** (*ee*AChE IC_{50} = **1.168 ± 0.723** μM) showed better inhibition as compared to other substituents. Conversely, the compound bearing aryl substitutions without any carbon linkers (**39-42**) and with one carbon linker (**43**) exhibited potent ChEs inhibitory profiles. Compound **39** (*ee*AChE IC_{50} = **0.886 ± 0.068** μM) and compound **43** (*ee*AChE IC_{50} = **0.806 ± 0.0431** μM; *eq*BuChE IC_{50} = **9.908 ± 0.017** μM) possessed the most significant inhibitory profile among all the synthesised derivatives. The excellent *eq*BuChE inhibition by compound **43**, indicating that one carbon linker in the compound bearing aryl substitutions i.e., *N*-benzyl piperazine is crucial for *eq*BuChE inhibition. The compound containing 2-pyridine ring on piperazine (**39**) showed excellent AChE inhibition but not active against BuChE. To further demonstrate inhibition of AChE, lead

compound **39** was additionally evaluated in an enzyme kinetic assay on *ee*AChE (113). The Lineweaver−Burk double reciprocal plot was used to elucidate the type of inhibition. In this experiment, reciprocal of the substrate [S] vs reciprocal of velocity [V] curves were plotted upon addition of different concentrations of inhibitor in the presence of five different substrates [S] concentrations to probe into the mechanism of ChEs inhibition. As depicted in **Figure 4.2A** by Lineweaver–Burk reciprocal plots, compound **39** displayed a mixed type of inhibition on *ee*AChE. Inhibitory concentrations (Ki) on *ee*AChE (0.25 µM) were calculated with the help of Dixon plot (**Figure 4.2B**).

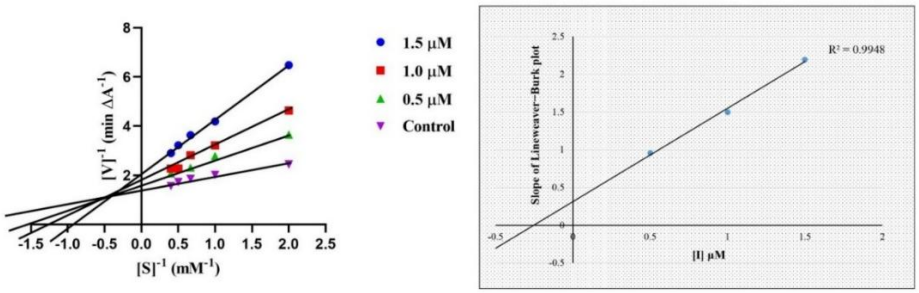

Figure 4.2: (A) Lineweaver-Burk plot for the kinetic study of *ee*AChE inhibition by compound **39 (B)** Dixon plot of compound **39** showing the Ki value as negative intercept on X-axis of the Dixon plot for AChE**.**

4.3.3 *In-vitro* blood-brain barrier permeation assay

The blood-brain barrier permeability is the major prerequisite of target molecules for the diagnosis or treatment of the AD. The BBB permeability of the potent ChEs inhibitors (**20**, **23**, **24**, **39**, **41**, **42** & **43**) assessed by parallel artificial membrane permeation assay (PAMPA) as described previously (113). The permeability of nine commercially available drugs reported earlier was used as a benchmark to establish the correlation between experimental Pe (exp) and evaluated for BBB permeability (Pe) (126, 135). The Pe values of tested compounds are listed in **Table 4.1**. Among the tested compounds, aryl substituted compounds (**39** & **41-42**) showed good BBB permeability within the CNS permeability cut-off values. The carbonyl containing CF_3 substituted compound **23** also

showed the appreciable BBB permeability **(Pe = 6.57 ± 0.075),** attributed to the presence of highly lipophilic trifluoromethyl (4-CF3) substituent at terminal phenyl group. Moreover, compound bearing the electron withdrawing groups (-OCH3) (compound **42**; **Pe** = **9.10 ± 1.880**) showed excellent BBB permeability among all the tested derivatives.

Table 4.1: Structures, cholinesterase inhibitory potential and PAMPA-BBB assay of tested compounds.

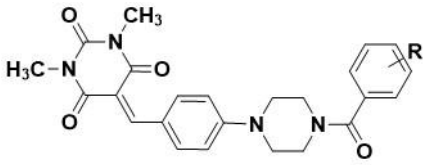

(18-28)

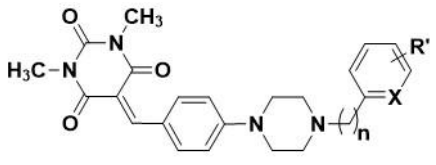

(39-43)

Com. No.	R	n	R'	X	IC_{50} (μM)[a] or % Inhibition ± SD		Pe (10^{-6}cm s^{-1})
					*ee*AChE	*eq*BuChE	
18	2-I	-	-	-	1.368 ± 0.947	n.a	-
19	2-OMe, 5-Cl	-	-	-	1.803 ± 0.842	14.71 % ± 0.638	-
20	4-OCF_3	-	-	-	1.550 ± 1.187	n.a.	2.50 ± 0.040
21	3-Br	-	-	-	1.168 ± 0.723	11.38 % ± 0.319	-
22	3-F	-	-	-	2.290 ± 0.389	n.a.	-
23	4-CF_3	-	-	-	1.183 ± 0.423	n.a.	6.57 ± 0.075
24	3-CN	-	-	-	1.631 ± 0.079	n.a.	2.85 ± 0.015
25	2,4-Cl	-	-	-	1.285 ± 0.104	18.73 % ± 1.770	-
26	H	-	-	-	1.862 ± 0.697	n.a.	-
27	3-NO_2, 4-Cl	-	-	-	1.877 ± 0.143	n.a.	-
28	2-Cl	-	-	-	2.516 ± 1.356	n.a.	-
39	-	0	H	N	0.886 ± 0.068	n.a.	4.83 ± 0.335
40	-	0	H	C	1.805 ± 0.689	n.a	-
41	-	0	4-F	C	1.136 ± 0.091	23.57 % ± 0.255	5.63 ± 0.435
42	-	0	4-OMe	C	1.163 ± 0.571	n.a	9.10 ± 1.880
43	-	1	H	C	0.806 ± 0.043	9.908 ± 0.017	4.11 ± 0.370
DPZ	-	-	-	-	0.073 ± 0.002	-	14.97 ± 1.96
RIVA[c]	-	-	-	-	-	0.87 ± 0.059	-

[a] IC_{50}: 50 % inhibitory concentration (mean ± SD of two or three independent experiments).

[b] Compounds with Pe > 4.324 × 10^{-6} cm s^{-1} could cross the BBB (CNS+). Compounds with Pe < 1. × 10^{-6} cm s^{-1} could not cross the BBB (CNS-), and compounds with 1.846 × 10^{-6} cm s^{-1} < 4.324 × 10^{-6} cm s^{-1} show uncertain BBB permeation (CNS±). [c]Rivastigmine.

4.3.4 Measurement of photophysical properties

The fluorescent properties, including, absorbance, excitation, and emission of the probes were evaluated. Interestingly, for probe **39**, as shown in **Figure 4.3,** the broad absorption spectrum was observed in PBS (10% DMSO) i.e., in the most polar solvent with maxima at 440 nm and emission spectrum with maxima displayed at wavelength of 640 nm. Then, the solid-state photoluminescence (PL) emission measurement was carried out to record the emission spectrum. The strong shift in the red region at wavelength of 663 nm was observed in the solid-state emission spectrum of probe **39 (Figure 4.3**). The relative fluorescence quantum yield of probe **39** in methanol was found to be 0.17. Further, solvatochromism studies of probe **39** were performed to evaluate the exact spectral characteristics, the absorption, excitation, and emission spectra of in different solvents **(Figure 4.3B & C**). Emission maxima (λ_{emm} in nm) of probe **39** displayed solvent dependency changes at certain extend in emission wavelength. The emission maxima in the spectra were observed in between 530-550 nm with distinct fluorescent intensity in the different organic solvent except water. Interestingly, only in the most polar solvent i.e., H_2O the shortest λ_{abs} (nm) of 440 and the longest λ_{emm} (nm) of 640 were observed with higher intensity. It may be due to the ongoing ICT transition with an increased dipole moment in the excited state compared to that of ground state.

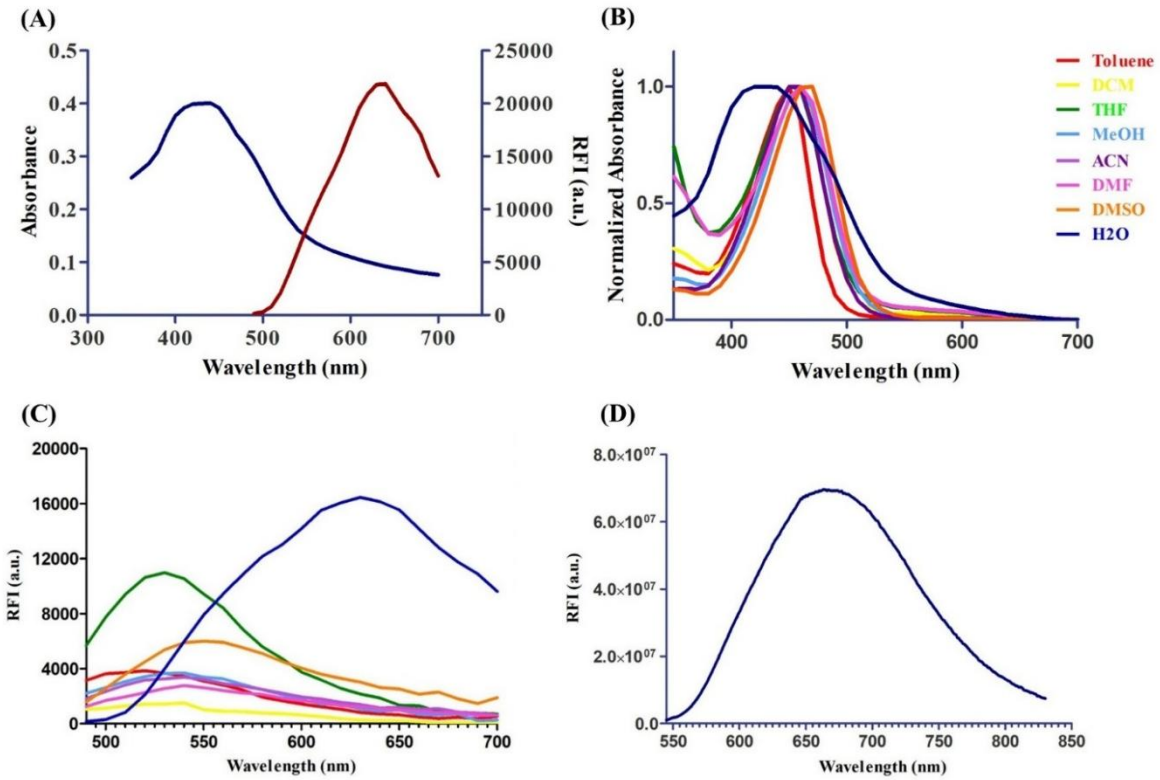

Figure 4.3 The absorption spectra and fluorescence emission spectra **(A)** of probe **39** in PBS (10% DMSO). The absorption spectra **(B)** and fluorescence emission spectra **(C)** of probe **39** in different solvents. Solid-state emission spectrum of probe **39 (D)**.

4.3.5 Binding studies with $A\beta_{1-42}$ aggregates

Fluorescent Aβ-binding probes should significantly change its fluorescence properties upon binding to Aβ aggregates (114). The formation of Aβ aggregates was accessed by Thioflavin T (ThT) assay (**Figure 4.4A**) (136). The change in the fluorescence response of probe **39** was accessed upon binding to $A\beta_{1-42}$ aggregates (**Figure 4.4B**). The fluorescent properties of free probe **39** in the aqueous solution (PBS) and their fluorescence properties in the presence of $A\beta_{1-42}$ aggregates were compared. A significant enhancement in the fluorescence intensity was observed upon association with $A\beta_{1-42}$ aggregates. The increase in intensity was observed at emission wavelength of 660 nm. The fluorescence enhancement in the emission spectra could possibly show that probe **39** would bind to the hydrophobic pockets of $A\beta_{1-42}$ aggregates and restricted its mobility.

The findings also suggested that probe **39** would produce "turned on" effect upon interacting with an $A\beta_{1-42}$ aggregates.

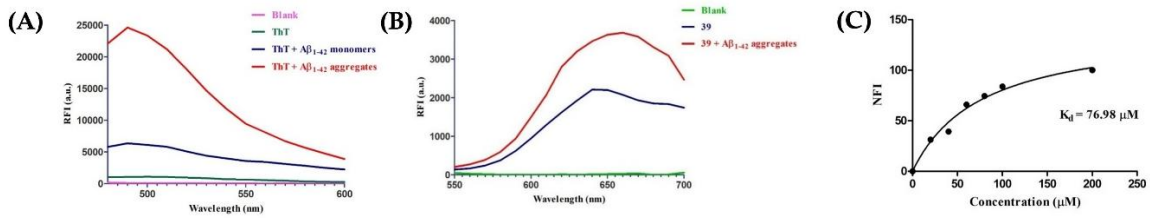

Figure 4.4: **(A)** ThT-fluorescence assay to confirm the formation of Aβ aggregates from Aβ monomers. **(B)** Emission spectra of probe **39** upon interaction with Aβ aggregates. **(C)** Binding constant of **39** toward the Aβ aggregates.

4.3.6 *In vitro* saturation binding assay using $A\beta_{1-42}$ aggregates

In order to quantitatively evaluate the binding affinity of probe **39** with $A\beta_{1-42}$ aggregates, an *in vitro* saturation-binding assay was conducted by the fluorescence titrations and the binding constant (**K_d**) constants were measured by using saturation assays (137, 138). As shown in (**Figure 4.4C**) the nonlinear curve fitting indicated that, probe **39** possessed high binding affinity toward the $A\beta_{1-42}$ aggregates with the apparent binding constant of **K_d** = 76.98 μM.

4.3.7 *In situ* fluorescence imaging of Aβ aggregation

In order to investigate and validate the binding affinity of probe **39** with Aβ aggregates, we performed fluorescence imaging for *in-situ* visualization of Aβ aggregation (139, 140). The prepared aggregated $A\beta_{1-42}$ peptide was established with the commonly used ThT fluorescence assay (**Figure 4.5**). The ability of the probe **39** to stain/bind the Aβ was accessed by co-localization of Aβ aggregate with ThT dye. At first, the ThT dye and Probe **39** was incubated separately with Aβ aggregates solution to access its ability to stain the Aβ aggregates and imaged using home-built wide-field epifluorescence microscope setup with respective filters and excitation sources. The emission from ThT was imaged using a bandpass filter (435−485 nm: ThT channel) upon excitation at 405

nm, whereas 488 nm excitation was employed for probe **39** bound Aβ aggregates imaging via the collection of emission between 590−700 nm (near IR channel). As shown in **Figure 4.5A & B**, ThT and Probe **39,** both showed the ability to stain the *in situ* Aβ aggregates. Further, the solution of Aβ aggregate in PBS was incubated together with probe **39** and ThT to image the colocalization. As shown in **Figure 4.5C & D**. The obtained results indicated that like ThT, probe **39** could stain the Aβ aggregates in the same manner, which was consistent with the result of above findings.

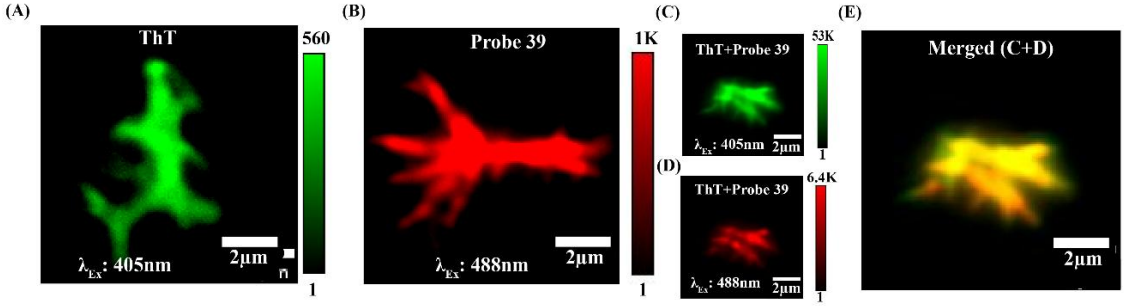

Figure 4.5: Fluorescence image of Aβ aggregates incubated with **(A)** ThT dye (emission filter: 435-485 nm, λ_{ex}: 405nm) and **(B)** probe **39** (emission filter: 590-700 nm, λ_{ex}: 488nm). Co-staining of Aβ aggregates with ThT and probe **39** imaged in **(C)** ThT channel (emission filter: 435-485 nm, λ_{ex}: 405nm) **(D)** Near IR channel (emission filter: 590-700 nm, λ_{ex}: 488nm) **(E)** Merged image of C and D.

4.3.8 Fluorescence lifetime measurement

Some fluorescent dyes show the ability to modify their fluorescence response with changes in the polarity of the environment (141). The mechanism can be applied with the increase in the hydrophobicity during the formation of the Aβ aggregates, where the change in fluorescence response observed (142, 143). Moreover, available reports also showed an increase in the fluorescence intensity along with the fluorescence lifetime when the environment of the dye changes from hydrophilic to hydrophobic (144, 145). Distinct from the fluorescence intensity, fluorescence lifetime measurement mainly depends on the inherent photophysical properties of each sensor that can effectively provide more accurate detection results (146). It provides several advantages including,

concentration independence that avoids the disturbance of fluctuation in probe concentrations, photobleaching, absorption, and excitation intensity, therefore it provides unambiguous assessment of micro-viscosity as well as polarity or hydrophobicity (145). The fluorescence lifetime of the probe **39** was measured with and without Aβ using TCSPC. The normalized average decay curve of the probe **39** alone and probe **39** incubated with Aβ was recorded as shown in **Figure 4.6A**. The calculated average lifetime for the probe **39** without Aβ was found to be 5.97 ± 0.20 ns. Whereas, for the probe **39** with Aβ, the average lifetime enhanced to 10.00 ± 1.12 ns, indicating the presence of Aβ bounded by probe **39**. Further, advanced fluorescence imaging techniques as FLIM was used to measure the fluorescence lifetime that also allowed visualization of Aβ aggregates when bound with the probe (146). As shown in **Figure 4.6B & C**, in accordance with TCSPC, the FLIM imaging showed the substantially longer lifetime for the probe **39** bound to Aβ aggregate with an average lifetime of 11.53 ± 0.01 ns as compared to probe **39** alone (6.92 ± 0.01 ns). The distribution of lifetime and decay curve of probe **39** with and without Aβ aggregates, analysed with SymphoTime software from FLIM data have been shown in **Figure 4.7.** Taken together, the results indicated that the probe **39** bounded/stained with Aβ exhibited the substantial increase in the fluorescence lifetime and signified the binding affinity of probe **39** towards Aβ aggregate. The enhancement in the fluorescence lifetime of probe **39** when bound to Aβ aggregates may be due to the binding of probe **39** to the hydirophobic pockets of $A\beta_{1-42}$ aggregates that restricted its mobility that leads to significant reduction of non-radiative pathways. The interesting characteristics of probe **39** makes it a potential candidate as a marker for Aβ aggregates.

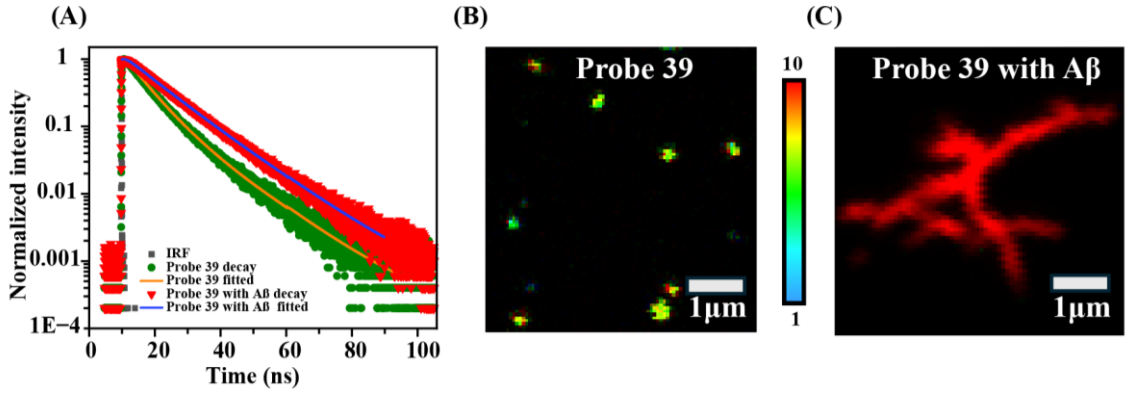

Figure 4.6: Fluorescence lifetime measurement. **(A)** Decay curve of the probe **39** incubated with Aβ (red curve) and without Aβ (green curve) obtained from TCSPC (λ_{ex}: 440 nm). **(B)** Average lifetime image of the probe **39** alone (λ_{ex}: 440 nm, emission filter: 590-700 nm). **(C)** Average lifetime image of Probe **39** incubated with Aβ aggregates (λ_{ex}: 440 nm, emission filter: 590-700 nm).

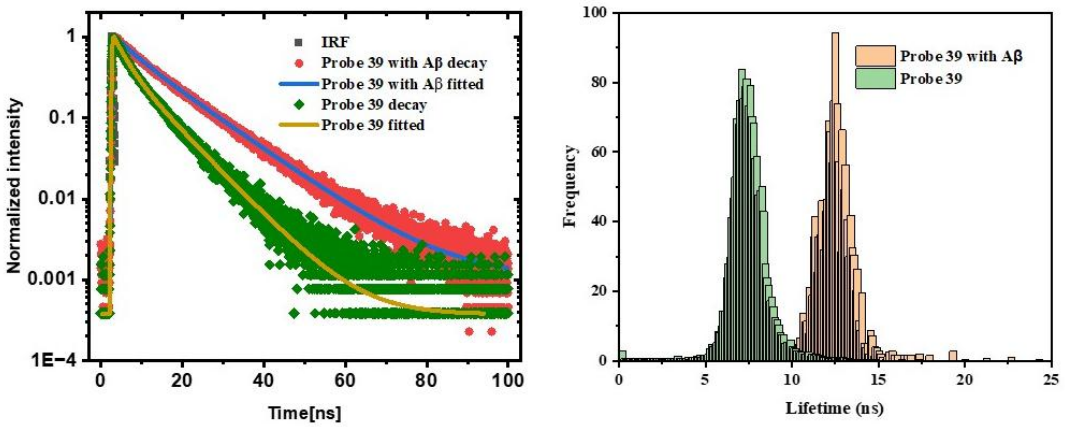

Figure 4.7: Lifetime distribution and decay curve of Probe **39** with and without Aβ obtained from FLIM analysis.

4.3.9 Density Functional Theory (DFT) calculation

DFT calculations were used to understand the relationship between fluorescence characteristics and structure of the probe. Frontier molecular orbital (FMO) of the probe is displayed in SI, **Figure 4.8**. In the highest occupied molecular orbital (HOMO) of probe **39**, electron cloud was mainly distributed on the pyridine and piperazine moieties i.e. donor region. While in the lowest unoccupied molecular orbital (LUMO), the electron cloud shifted on the 1, 3-dimethylbarbituric acid moiety i.e. acceptor region of probe. The results indicated that the probes could possess charge transfer delocalisation phenomena

in the D–π–A type scaffold (71, 147). The lower energy gaps, ΔE = 3.3556 eV between these orbitals indicates the high reactivity of the developed probe **39**.

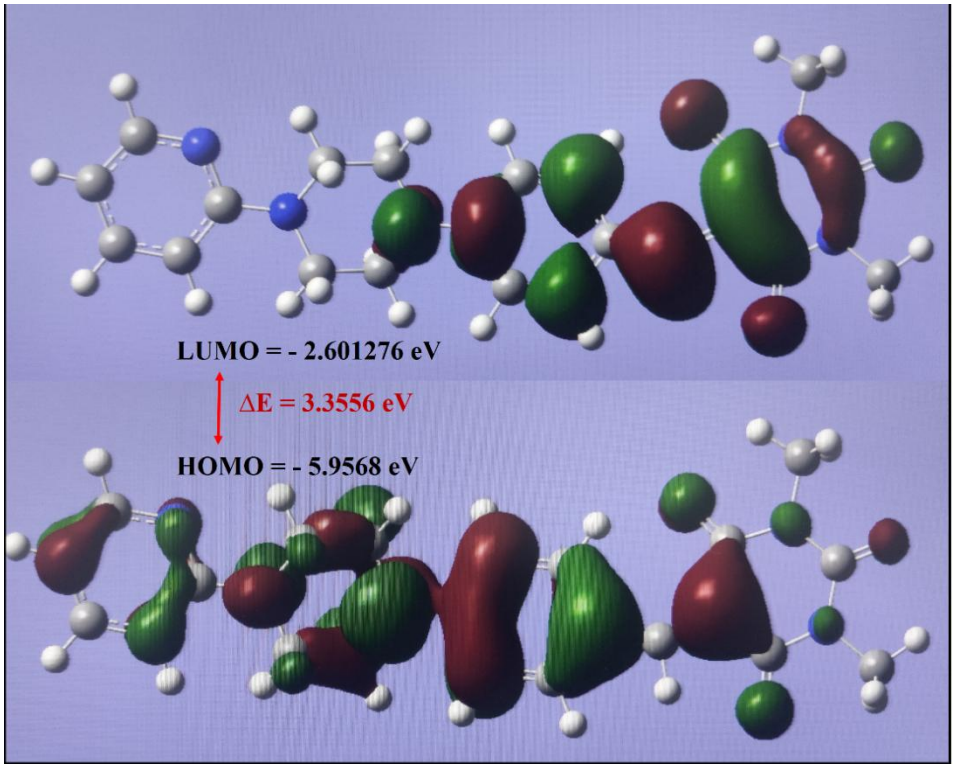

Figure 4.8. Probe frontier molecular orbital.

4.3.10 Molecular docking analysis

Molecular docking studies of final lead **39** was performed to validate the design strategy and gain an insight into the binding mechanism with respective targets. The binding behavior of compound **39** towards both the AChE (**4EY7**) and $A\beta_{1-42}$ species (**5OQV**) proteins, was investigated. The active sites of the AChE located at the bottom of a narrow gorge consisted of an anionic site (AS) (Trp86), esteratic site (Ser203, Glu334, and His447), and PAS, i.e., peripheral anionic site (Tyr72, Asp74, Tyr124, Trp286, and Tyr341) (132). As per the obtained interaction in molecular docking studies, compound **39** effectively interacted with residues of the esteratic site and PAS site of AChE (**Figure 4.9).** The 1, 3-Dimethylbarbituric acid moiety primarily established the hydrogen bonding interaction with principal residues of the esteratic site, i.e., Ser203 and His447. The bridge between the donor and acceptor region including piperazine and barbituric

acid scaffold involved in the interaction with the PAS residues including Trp286 along with Phe338 and Tyr341 through π-π stacked and π alkyl interaction, respectively. *N*-aryl piperazine scaffold actively formed the π-alkyl interaction with residue of Leu289 and Val294 along with π-donor H-bond interaction with Ser293. Furthermore, promising results were also observed in the binding mode interaction of compound **39** with $A\beta_{1-42}$ species (**Figure 4.10**). The potential binding sites of Aβ species represented as A, B, and C sites that have been reported for the designing of the probes. The sites A and B locates at hydrophilic N-terminal portion and the hydrophobic mid-region respectively, whereas, C site formed by a hydrophobic C-terminal from one Aβ peptide and hydrophilic N-terminal from another Aβ peptide (31, 148). Despite having only, the difference of two amino acids between $A\beta_{40}$ and $A\beta_{42}$ species, distinct hydrophobicity of $A\beta_{40}$ and $A\beta_{42}$ makes the $A\beta_{42}$ much stickier and considerably easier to aggregate. Whereas, site C was considered as the suitable region for designing probes to differentiate $A\beta_{40}$ and $A\beta_{42}$ species. At site C, where multiple pieces of the Aβ peptide formed a gulf, in which one of the sides consisted of hydrophobic amino acids of Val39, Val40, Ile41, and Ala42 (isoleucine–alanine), the last two amino acids in $A\beta_{42}$ species (31). Among them 1, 3-Dimethylbarbituric acid moiety and aromatic ring bridge of compound **39** bound with the Val39, Val40 and Ile41 with H-bonding, π sigma and π alkyl interaction respectively. Therefore, it showed the potential to differentiate the $A\beta_{40}$ and $A\beta_{42}$ species. The *N*-aryl piperazine scaffold involved in the interaction through H-bond with Gly 29 and π sigma and π alkyl interaction with Lys28 & Ala30, respectively.

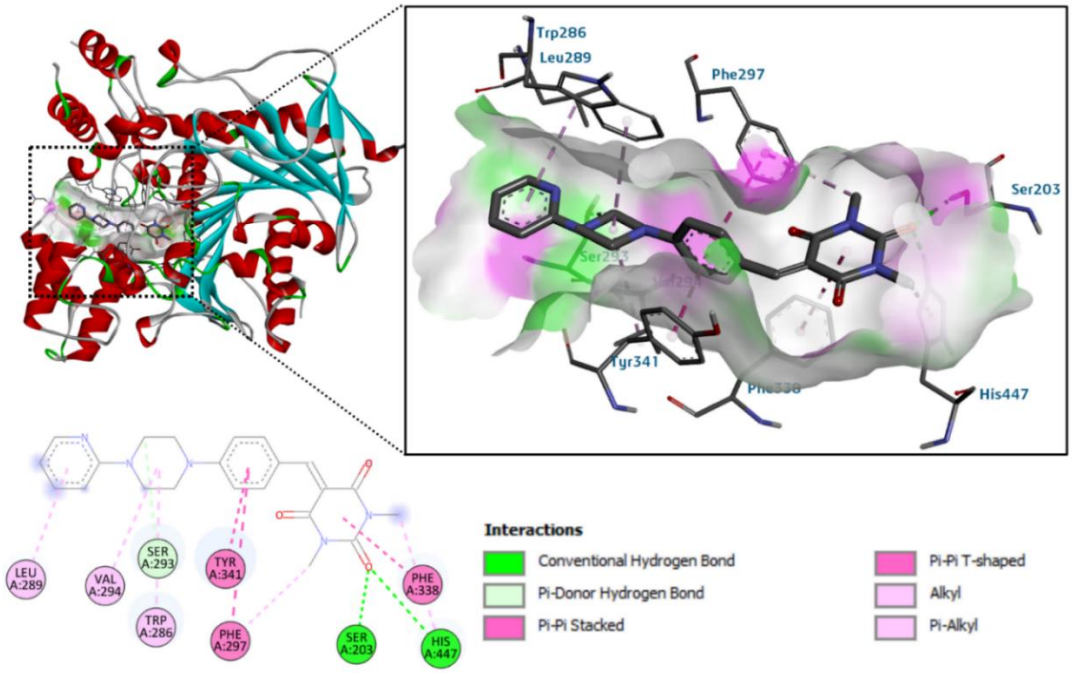

Figure 4.9: Binding interaction mode of compound **39** with AChE (PDB: **4EY7**).

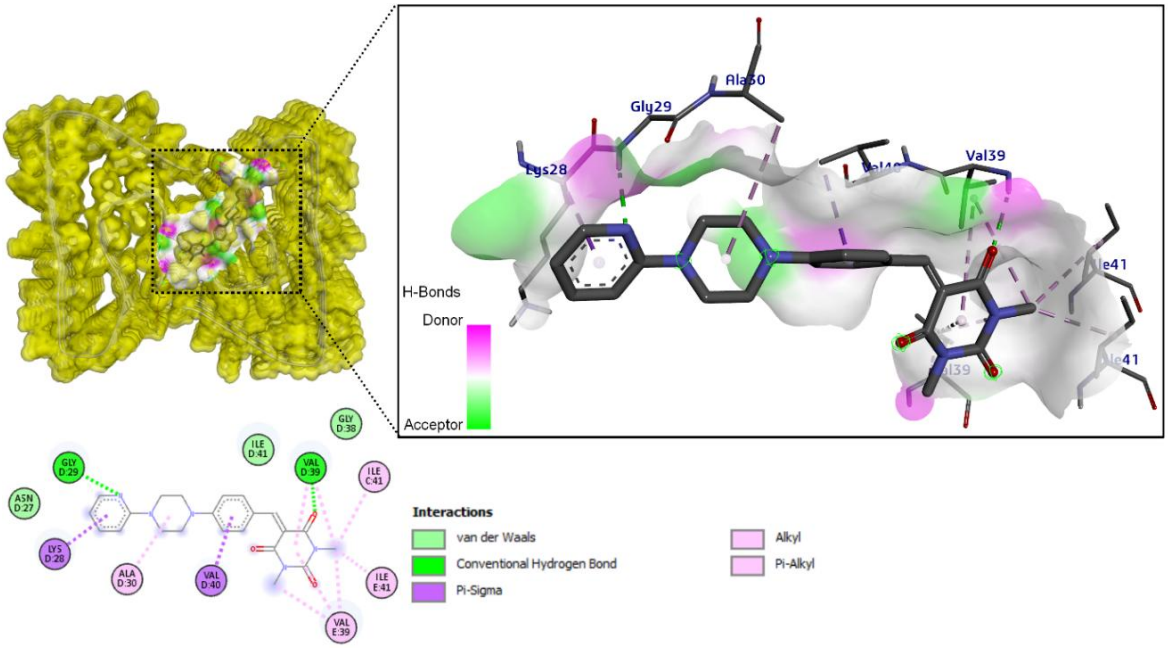

Figure 4.10: Binding interaction mode of compound **39** with Aβ species (PDB: 5OQV).

4.3.11 *In vivo* biological evaluations

4.3.11.1 Acute toxicity studies

The acute oral toxicity studies of the most promising compound **39** were performed to assess its safety profile in female mice as per the OECD guideline 423. The obtained results demonstrated no sign or symptoms of any toxicity effects and no change in body weight, food, and water intake, no mortality was observed on the administration of compound **39**. Compound **39** did not show any histological damage in the animal organs including, brain, liver, heart, or kidneys in histological assessment up to 300 mg/kg dose (**Figure 4.11**).

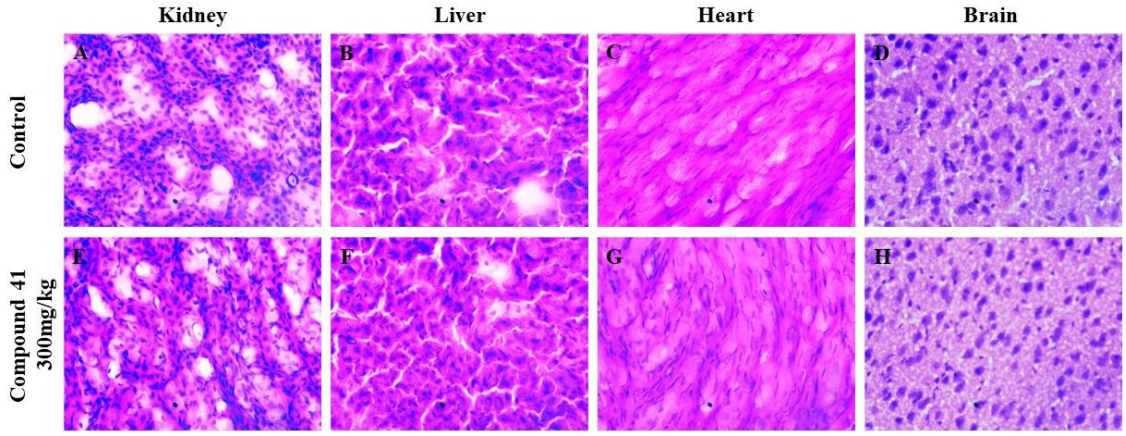

Figure 4.11. Effect of compound **39** (300 mg/kg) on organ toxicity. Histological examination (**A–D**) Control group without treatment effect on kidney, liver, heart, and brain, respectively. (**E–H**) Effect of compound **39** on histological abnormalities in kidney, liver, heart, and brain, respectively.

4.3.11.2 Behavioural studies

The *in vivo* therapeutic potential of the compound **39** was evaluated with behavioural studies and accessed the ability to ameliorate cognitive dysfunction and effect on the improvement of memory in scopolamine-induced cognitive deficit mice model (123). The Y-maze test is frequently employed in studying cognitive function, particularly in experimental models involving scopolamine-induced cognitive deficits. This test

evaluates short-term spatial working memory, utilizing the natural exploratory behavior of mice in a maze with three arms to gauge spontaneous alternation. It's widely used to measure cognitive function in mice treated with scopolamine, a cholinergic antagonist that induces memory impairment. Additionally, the Y-maze test (scopolamine-induced amnesia model) is adopted to assess the effectiveness of potential therapeutic agents in ameliorating memory deficits induced by scopolamine in animal models (149). The specified dose of scopolamine is commonly used to study the cognitive dysfunction owing to its ability to cause cholinergic deficiency (150). The Y-maze test was used to determine the % alternation or spatial working memory in the scopolamine-induced memory impairment treated with compound **39** (151, 152). The activity of spontaneous alternation behaviour of the lead compound **39** with dose of 5, 10, and 20 mg/kg was evaluated using DPZ (5 mg/kg) as reference standard (**Figure 4.12**). The measurement of sequential arm entries and score of % spontaneous alternations were carried out along with the total number of arm entries of respective animals (**Figure 4.12**). Significant differences were observed among all the animal groups as evident from one-way annona. The notable decrease in the % spontaneous alternations ($p < 0.05$) in the scopolamine-treated group was observed as compared to that of control group. However, the compound **39** and DPZ treated group showed significant increase in the % spontaneous alternation as compared to scopolamine group. Statistically significant difference was observed in compound **39** treated group at a dose of 5 mg/kg, 10 mg/kg and 20 mg/kg in spontaneous alternation as compared to scopolamine group. On the other hand, compound **39** at doses of 20 mg/kg, did not show any significant difference ($p > 0.05$) in comparison to DPZ treated group. The above findings demonstrated that compound **39** has ability to improve memory deficit functions by producing remarkable improvement in the cognitive and memory function in the scopolamine-induced amnesia model.

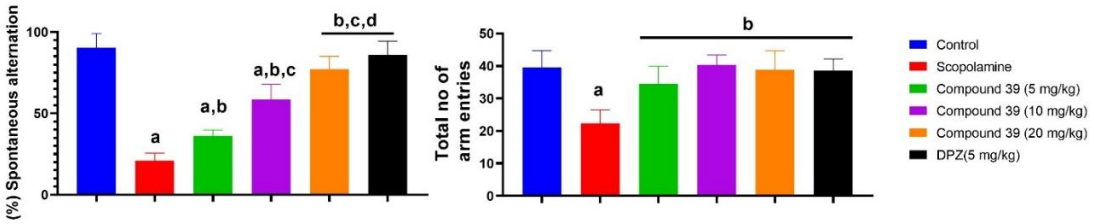

Figure 4.12 Effect of compound **39** and DPZ on cognition enhancement in the scopolamine-induced amnesia model. **(A)** Indicates % spontaneous alternation. **(B)** Indicates total no of arm entries. [a] $P < 0.05$ vs. control group; [b] $P < 0.05$ vs. scopolamine group; [c] $P < 0.05$ vs. compound **39** (5 mg/kg) group; [d] $P < 0.05$ vs. compound **39** (10 mg/kg). One-way ANOVA followed by Newman - Keuls posthoc test.

4.3.11.3 *Ex-vivo* biochemical analysis

The potential effects at neurochemical levels on treatment with compound **39** was observed on the estimation of the biochemical parameters including, levels of ACh and AChE along with oxidative stress biomarker levels of MDA and CAT. After completion of behavioural studies, experimental animals were sacrificed via cervical dislocation of the respective groups and brain hippocampal regions was isolated and then homogenized. The estimation of *ex vivo* level of ACh was determined using an ELISA kit and the level of AChE was assessed with modified Ellman's method (134). The obtained results demonstrated that the decreased levels of ACh and higher rates of substrate hydrolysis or increased in AChE levels in the scopolamine-treated group as compared to the control group ($p < 0.05$). Whereas, animals treated with compound **39** and DPZ had significant increase in the levels of ACh and decreased in the AChE levels or substrate hydrolysis as compared to that of scopolamine-treated animal group ($p < 0.05$). The assay finding also suggested the ability of compound **39** to cross the BBB, which resulted in increased ACh and decreased AChE levels. Further, brain homogenate of the animals treated with compound **39** were used to evaluate antioxidant properties. The levels of oxidative biochemical markers including, MDA and CAT were estimated. The obtained results indicated induced oxidative stress in scopolamine-treated mice group that showed significantly decreased levels in CAT and increased in the level of MDA as compared to

the respective control animal group ($p < 0.05$) (**Figure 4.13**). However, compound **39** treated group reduced the MDA levels while significantly increased the levels of CAT as compared to the scopolamine-treated animal group. The DPZ-treated group indicated the elevated level of CAT and significantly decrease in the MDA ($p < 0.05$). Thus, the findings from the *ex vivo* biochemical estimation suggested that compound **39** have the significant AChE inhibitory activity and potential to retard the oxidative stress induced by scopolamine.

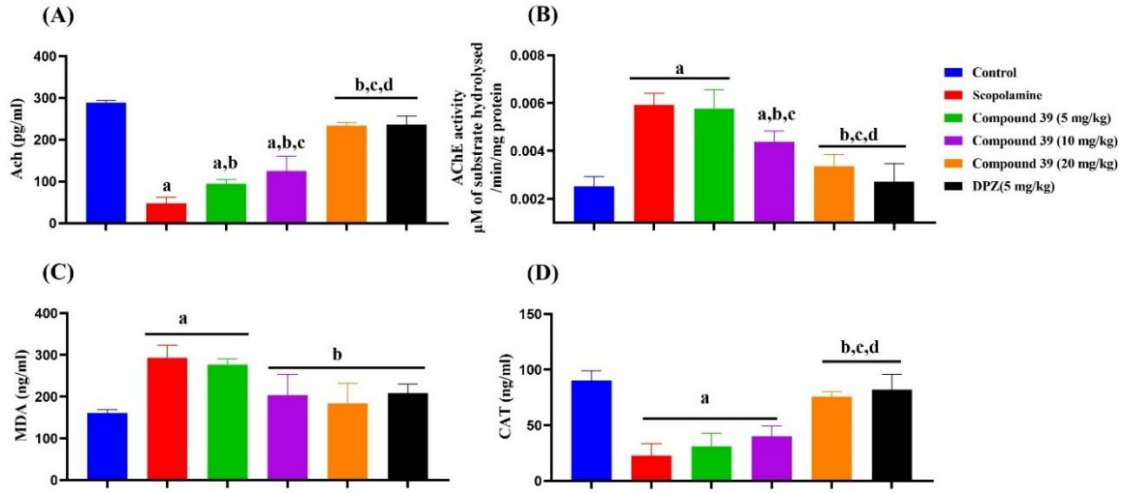

Figure 4.13. *Ex vivo* estimation of the effect of compound **39** on biochemical parameters. **(A)** ACh activity. **(B)** AChE activity, **(C)** Estimation of MDA activity and **(D)** CAT levels estimation. [a] $P < 0.05$ vs. control; [b] $P < 0.05$ vs. scopolamine; [c] $P < 0.05$ vs DPZ; [d] $P < 0.05$ vs. compound **39** (10 mg/kg).

4.4 Summary and conclusion

The theranostic agents for AD were designed through the amalgamation of structural features from the potential anti-AD agents and the fluoroprobes were constructed with the architecture of an electron donor-acceptor. The AChE and BuChE inhibition assays and structure-activity relationship studies showed all the tested compounds endowed with potential anti-cholinesterase activity. The optimal compound/probe **39** (*ee*AChE IC_{50} = **0.886 ± 0.068** µM) and **43** (*ee*AChE IC_{50} = **0.806 ± 0.0431** µM; *eq*BuChE IC_{50} = **9.908 ± 0.017** µM) exhibited potent inhibitory activities. The obtained results of BBB assay

using widely used parallel PAMPA model anticipated excellent BBB permeability (CNS+) of the lead compounds. Significant fluorescence emission profiles of the synthesized probes were observed on the measurements of different spectroscopic properties. In the binding study assay, probe **39** on binding with $A\beta_{1-42}$ aggregates, displayed enhancement in the fluorescence intensity. *In vitro* saturation binding assay proved a high affinity of probe **39** towards the $A\beta_{1-42}$ aggregates (K_d = **76.98** μM). Interestingly, the significant enhancement in the fluorescence lifetime of probe **39,** when in binding to Aβ aggregates, was observed with TCSPC and FLIM analysis. Moreover, the binding affinity of the probe **39** with $A\beta_{1-42}$ aggregates was validated on the basis of colocalization with ThT. The plausible fluorescence response mechanism of the probes was established by the DFT calculation studies. The computational binding mode analysis against AChE & Aβ species advocated the potential of probe **39** as theranostic agent. Acute toxicity studies demonstrated no sign of any toxicity and no changes in body weight or food and water intake and absence of mortality on the administration of lead compound **39**. In the *in-vivo* behavioural studies, lead compound **39**, at oral dose of 20 mg/kg, demonstrated a substantial improvement of the cognitive and special memory impairment in the scopolamine-induced cognitive deficit mice model. Further, the brain AChE inhibitory potential of lead compound **39** was affirmed through *ex vivo* biochemical analysis with reduced AChE and increased ACh levels along with strong antioxidant potential. In addition to the excellent properties as contrast fluorescent agent, both *in-vitro* and *in-vivo* investigations evidenced that compound **39** has potential, is safe and effective lead for AD. To our knowledge, this is the first theranostic fluorescent probe developed for simultaneously detection of the Aβ aggregates and to inhibit the cholinesterase enzymes, which are primary targets for the development of therapeutics for AD.